Stockholm University

Master Thesis

Degree Project in Geology 30 hp

Thermal and chemical variations in metamorphic rocks in Nautanen, Gällivare, Sweden

Elin Tollefsen

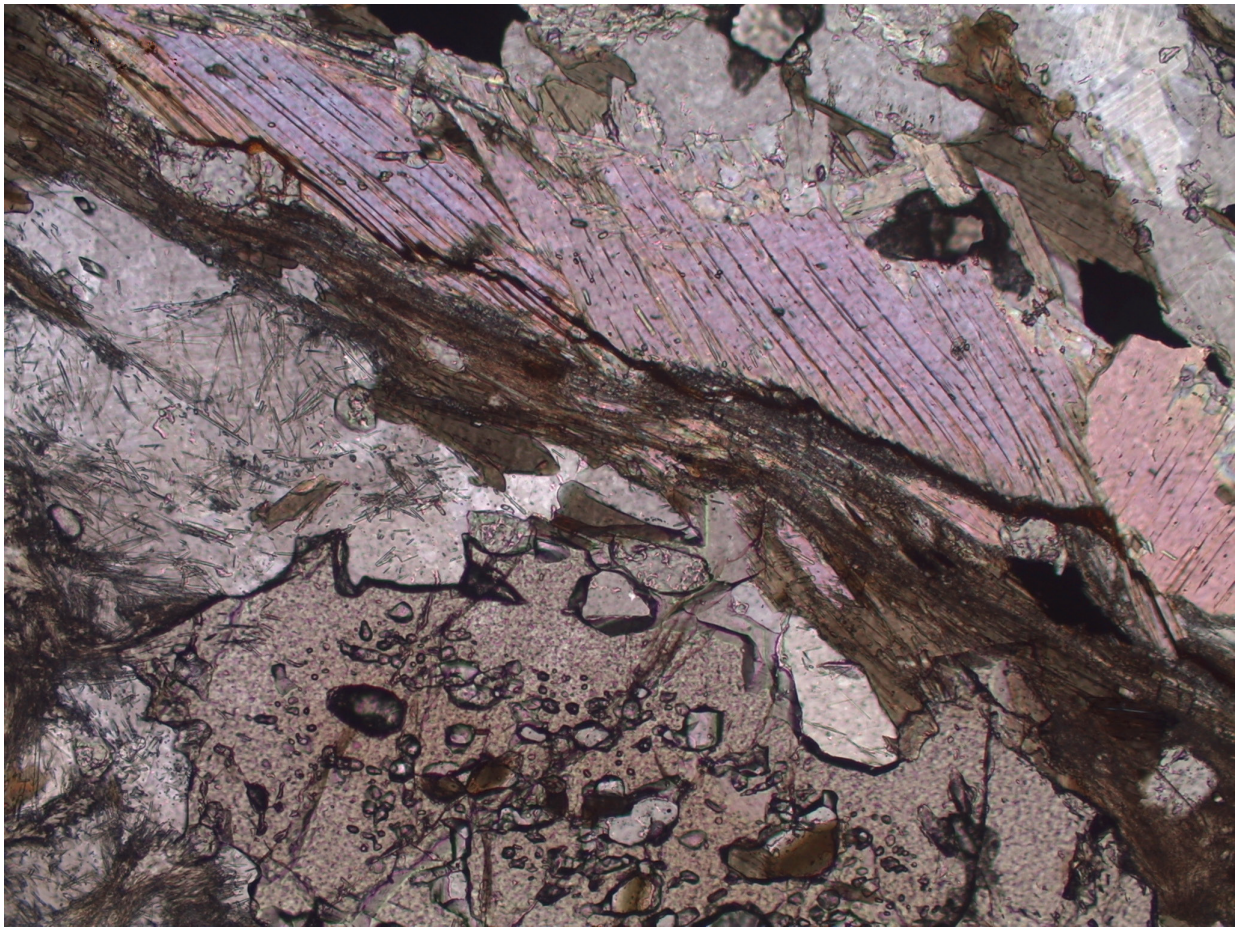

Stockholm 2014

Department of Geological Sciences
Stockholm University
SE-106 91 Stockholm

Abstract

This study focuses on the geology of the Nautanen area. It is part of the SGU-financed project, Metamorphic Map of Sweden, which aims to compile metamorphic data from Sweden and takes the form of a number of Bachelor and Master projects. The main metamorphic event in the Nautanen area is the Svecokarelian Orogeny (1.96 – 1.75 Ga). The samples are metamorphosed sedimentary and volcanic rocks, which were intruded by intermediate to mafic intrusions and a later granite intrusion. The supracrustal rocks are folded and the Nautanen Deformation Zone (NDZ) traverses the area in a NW to SE direction. Petrographic studies, XRF analysis and THERMOCALC were used to estimate pressure and temperature and to elucidate evidence of fluid mobility. The average pressure was assumed to be below 4 kbar because of the presence of andalusite. The lowest and highest temperatures for metamorphism were 474±43°C and 681±14°C, with highest temperatures recorded nearest to the granite intrusion. XRF analysis revealed high concentrations of Ba (up to 7000 ppm) in the NDZ. High concentrations of Ba, skarn formation and replacement of garnet by chlorite indicate fluid-controlled metamorphism in the NDZ. The increasing temperature towards the granite intrusion suggests regional or contact prograde metamorphism that need not be related to the NDZ.

Contents

Introduction 3
Geological background and tectonic history 4
Method 7
Thin section 7
XRF 7
SEM 8
EMPA 8
THERMOCALC 8
Results 9
Petrographic study 9
West of the NDZ 11
Locality 4 12
Locality 10 14
East of the NDZ 14
Locality 12 14
Locality 13 15
Central part of the NDZ 17
Locality 17 17
Locality 18 18
Locality 11 19
Locality 3 21
Locality 1 21
Geochemical results 23
Results from THERMOCALC 27
Discussion 29
Petrology 29
THERMOCALC 32
Geochemistry 33
Uncertainties 33
Conclusion 34
Acknowledgement 34
References 35
Appendix 38
Appendix A 38
Appendix B 43
Appendix C 46

Introduction

The Svecokarelian orogen took place at around 1.96 - 1.75 Ga. The metamorphism and the ore formations resulting from this event are visible in a large part of Sweden (Fig. 1). The purpose of this study is to investigate the metamorphic history in Nautanen, a small area close to Gällivare in Norbotten County. Nautanen is traversed by a major deformation zone, the Nautanen Deformation Zone (NDZ). The area was first studied by Per Geijer (1918). Since then several studies have been conducted in the area, mainly on the Aitik deposit situated south-west of the NDZ (Zweifel 1976; Martinsson et al. 2004; Wanhainen et al. 2012). Few studies have previously been done on the metamorphism in Nautanen. In a paper from Bergman et al. (2001) the metamorphism in Norbotten County is briefly described. The metamorphic grades attributed to different area are from compiled information from earlier publications and from studies by the authors.

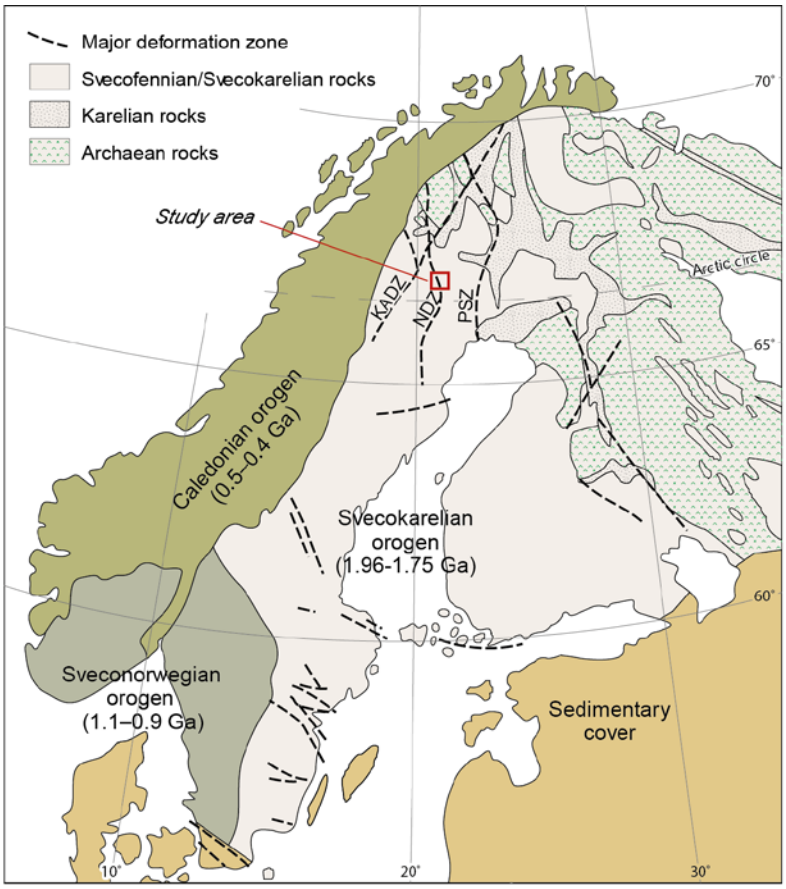

Fig. 1 Major geological units in the Fennoscandian Shield and surrounding areas. Modified from Gorbatschev & Bogdanova (1993, Olesen & Sandstad (1993), Stephens et al. (1994), Korsman et al. (1997) and Bergman et al. (2001). KADZ = Karesuando-Arjeplog Deformation Zone, NDZ = Nautanen Deformation Zone, PSZ = Pajala shear zone. The study area is shown by a red square.

Bergman et al. (2001) define the metamorphic grade based on the classification from Winkler (1979); low grade may contain chlorite and epidote; medium grade may contain andalusite, prograde muscovite, garnet and cordierite; and high grade may contain sillimanite and K-feldspar, and no prograde muscovite. In Norbotten County, the three different grades are present; areas with low grade are found in the east, medium grade is found throughout the area, and high grade is mainly found in the east and the south. Metamorphic boundaries are located along fault zones or deformation zones (Bergman et al. 2001). The metamorphic grade in Nautanen according to Bergman et al. (2001) is medium grade in the deformation zone and high grade on both side of the deformation zone. The aim of this study is to provide a more

quantative estimate of metamorphic grade in the Nautanen area and to investigate the influence of the NDZ on metamorphism.

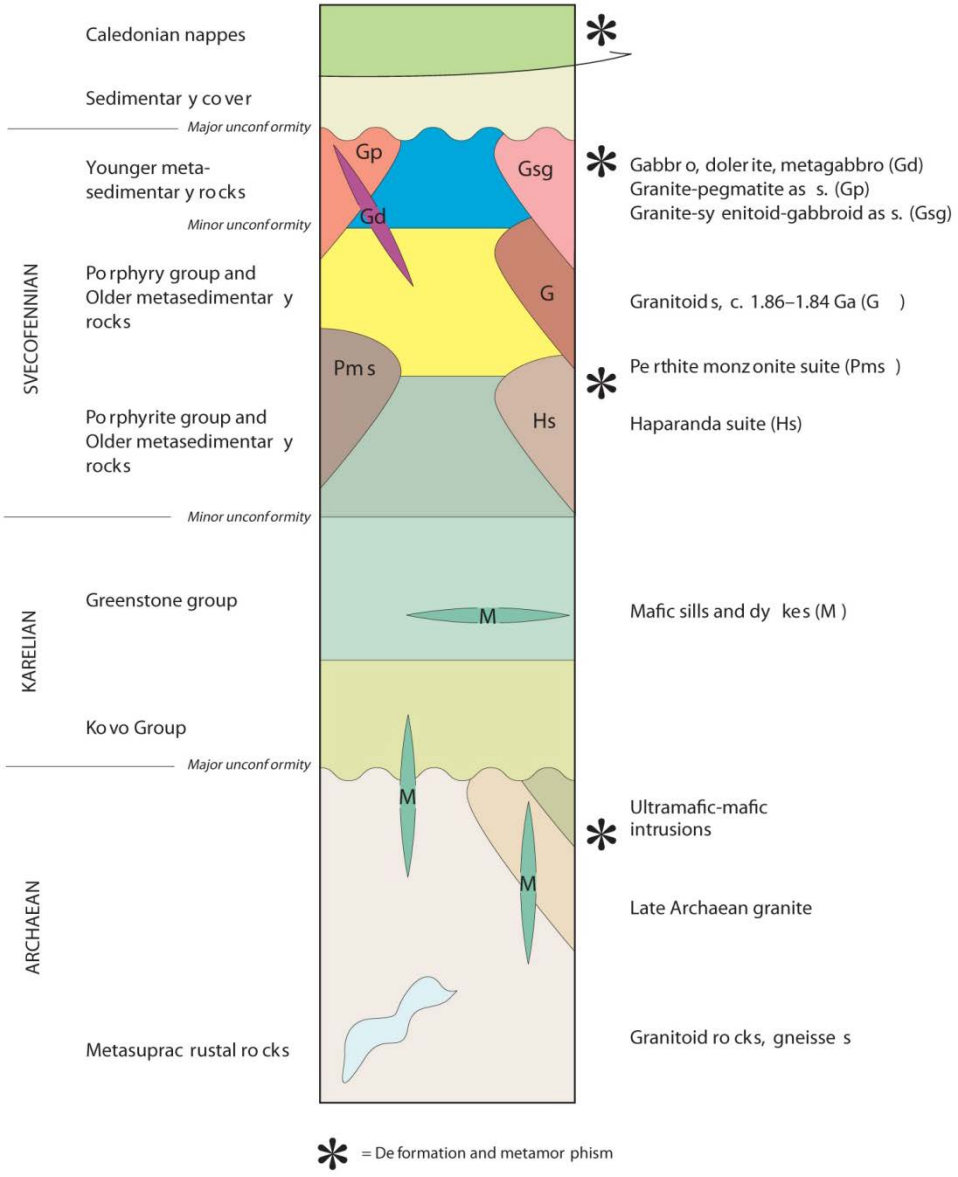

Fig. 2 Summary diagram with schematic illustration of main rock units and events in Norbotten County. Not to scale. The rocks in this study are part of the Svecofennian unit, the Porphyry group. From Bergman et al. (2001).

Geological background and tectonic history

The study area is situated on the Fennoscandian shield, which is the exposed Precambrian part of the larger East European craton (Fig. 1). The age of formation for these rocks is from 2.85 to 1.78 Ga (Bergman et al. 2001). In the north-west part of Norbotten, some Archean rocks are

visible. They are unconformably overlain by Karelian rocks. The Karelian rocks are mostly conformably overlain by Svecofennian supracrustal rocks (Fig. 2). In Nautanen, the supracrustal rocks are composed of metasediments and metavolcanics. These rocks have been dated to 1.91-1.88 Ga (Skiöld et al. 1984). The Nautanen rocks were first intruded by diorites from the Haparanda suite. The diorite has been dated to 1873±24 Ma (U-Pb zircon, SGU unpublished data). Thereafter the supracrustal rocks were intruded by a large granite intrusion (Lina granite) which has been dated to 1778±7 Ma (U-Pb ziricon SGU, unpublished data). The granite intrusion surrounds the Nautanen area and it is weakly foliated. When the granite is in contact with the more strongly foliated and earlier Haparanda suite intrusion the foliations are parallel. Therefore it is suggested that the granite intruded while deformation was still ongoing (Bergman et al. 2001). The supracrustal rocks are folded. A deformation zone, the Nautanen Deformation Zone (NDZ), traverses the folded rocks in a NW to SE direction.

The tectonic history of Norbotten is complex and still not fully understood. Isotope data indicates that Archean crust is below the Paleoproterozoic cover in the study area. The Archean - Protezoric boundary (Fig. 3) has been detected north of the Skellefteå area, where it is referred to as the Luleå-Jokmokk paleoboundary (Öhlander et al. 1999; Mellqvist et al. 1999). The main tectonic events that are significant for the study area are:

1. Continental rifting (Fig. 3) that took place on the Archean craton between 2.5 and 1.9 Ga (Weihed et al. 2005). A successful rift evolved in a NW-SE direction and a failed rift evolved in a NNE direction. The Archean margin of the successful rift acted as a passive margin during the opening of an ocean (Wanhainen et al. 2012).

2. At ca 1.93 Ga the regime changed and volcanic arc subduction took place. The subduction event reworked older crust and generated a large amount of juvenile Proterozoic crust. The Svecofennian supracrustal rocks formed in relation to northward subduction. They were deposited between 1910 and 1860 Ma (Skiöld 1984). The Haparanda suite intrusions were generated by the same event. They have been dated to 1.89 – 1.86 Ga (Skiöld 1987).

3. At c. 1.86 to 1.84 Ga there was a change in deformation intensity and in magmatic activity. This was possible due to a change in regime from collisional to continental extension (Bergman et al. 2001; Lahtinen et al. 2005).

4. The last stage of the Svecokarelian Orogeny was continent to continent collision at 1.84 – 1.79 Ga, the rocks were reworked and new magmas formed and intruded large part of Norbotten (Bergman et al. 2001; Lahtinen et al. 2005).

The Nautanen Deformation Zone (NDZ) traverses the area of interested in a NNW-SSE direction. East of the deformation zone is a synclinal fold. The fold is open and gently plunging to the SSE. On the west side of the NDZ there is a synform. The NDZ is one of several important deformation zones in Norbotten (Fig. 3). In the study area the NDZ is an approximately 1 km (northern part) to 3 km (southern part) wide zone with strong ductile deformation in a NNW-SSE direction (Bergman et al. 2001).

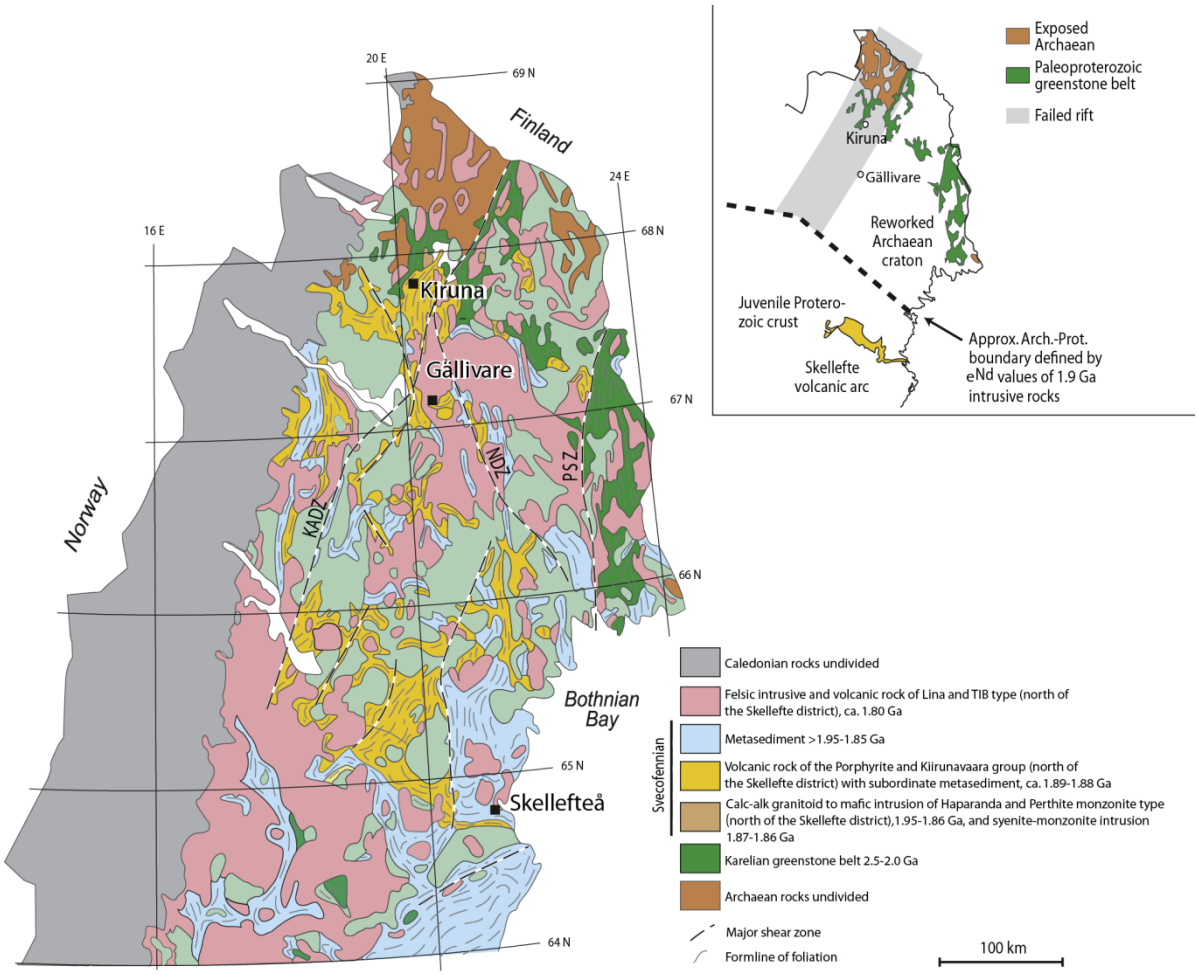

Fig. 3 General geology of northern Sweden. Insert shows location of the Archean-Proterozoric boundary and the failed rift. KADZ = Karesuando Arjeplog Deformation Zone, NDZ = Nautanen Deformation Zone, PSZ = Pajala Shear Zone. Modified from Weihed and Williams (2005) and Wanhainen et al. (2012).

The NDZ has been detected as a lineament from magnetic and gravity field data. The discontinuity is followed to a depth of over 5 km using geophysical data (Bergman et al. 2001). I have chosen these delimitations of the NDZ in my study and that is how the zone is delimitated on the simplified geological map over the study area (Fig. 4)

Analyses of titanite and allanite from the NDZ preserve evidence of a metamorphic event within the period 1800-1750 Ma probably during movement of fluid along the shear zone (Smith et al. 2009).

Close to and in the NDZ several epigenetic deposits have been discovered. On the west side of the NDZ is the open pit mine Aitik, one of Europe's most important copper and gold producers. Several small copper and gold mines were explored for a few years in the beginning of the 19th century in the NDZ and east of the zone (Geijer 1918). The deposits in the NDZ and in the western part of the study area are disseminated e.g. Aitik and Nautanen. East of the NDZ, the deposits are of vein-type e.g. Ferrum and Fridhem (Martinsson et al. 2004).

Method

Thin section

Forty-one samples of metasedimentary and metavolcanic rocks were collected in the study area. Of these, thirty-seven samples were selected as appropriated for the study. They were sawn, prepared and polished to make thin-sections at the Department of Geological Sciences, Stockholm University. Polished thin sections were made by Dan Zetterberg at Stockholm University and by Vancouver Petrographics in Canada. The mineralogy, texture and structural relationships in the thin-sections were studied using a petrographic microscope. Each thin-section was point counted to estimate the mineral proportions. One thousand points per thin-section were counted. The standard deviation (σ) for the counting of mineral proportions is calculated as follow:

$$\sigma = \sqrt{p(100-p)/n}$$

Where p = the real content of a mineral in percent by volume and n = the total number of points counted. This gives a maximum error of ±2 % for 1000 points counted (van der Plas and Tobi 1965).

XRF

Twenty-one samples were crushed and powdered for X-ray fluorescence (XRF) analysis of whole rock chemistry. The weighted and crushed samples underwent loss on ignition (LOI). The samples were first heated to 105˚C to remove excess water, and then heated a second time to 1000 ˚C to remove carbon and structural water. The samples were weighted again and the difference in weight is the LOI. After this the pulverized rocks were mixed with lithium metaborate flux at 5:2 ratios to facilitate fusing. The samples were fused to glass discs with a Phoenix autofuser. The XRF analysis was done with a Rigaku Primus II X-ray Fluorescence spectrometer at the Department of Geological Sciences, Stockholm University. Major elements and 16 trace elements were analysed.

SEM

Some thin-sections were analysed with Energy Dispersive X-ray (EDS) system to get the elemental composition of unknown minerals. This is one of the detectors of the Scanning Electron Microscopy (SEM) at the Department of Geological Sciences. The instrument at Stockholm University is an Environmental Scanning Electron Microscope with Field Emission Gun of the brand Philips XL-30- ESEM-FEG.

EMPA

An Electron Probe Microanalyser (EPMA) at Uppsala University was used to determine the chemical composition for selected minerals, the model is a Jeol JXA-8530F Hyperprobe. It is

equipped with four wave dispersive spectrometers (WDS) and can perform quantitative element analyses from Beryllium to Uranium. The beam current for the analyses was 10 nA, the voltage 15 kV and the spot size was 3 µm for feldspar, 2 µm for micas and 1 µm for all the other minerals. The thin sections were previously carbon coated to increase the electrical conductivity. The result was given as major oxide composition in weight percent for each mineral.

THERMOCALC

Single reactions are commonly used as geothermometers or geobarometers for a particular mineral assemblage in metamorphic petrology. For example one reaction that is commonly used as a geothermometer is Fe and Mg exchange between garnet and biotite:

$$KFe_3AlSi_3O_{10}(OH)_2 + Mg_3Al_2Si_3O_{12} = KMg_3AlSi_3O_{10}(OH)_2 + Fe_3Al_2Si_3O_{12}$$

biotite + garnet = biotite + garnet

These reactions are calibrated experimentally. Previous work led to a collection of standard calibrated reactions. THERMOCALC is a software tool developed by Roger Powell and Tim Holland in 1988. The software uses an internally consistent thermodynamic dataset (Holland and Powell 1998) to perform geothermobarometry calculations. The dataset has undergone various updates with new phase equilibrium constraints, calorimetry and new measurements of molar volume, thermal expansion and compressibility. The strength of THERMOCALC is to use all this information for all possible reactions to evaluate the P-T conditions for metamorphism recorded by a chosen mineral assemblage in a thin-section. If the minerals are considered to have once been in equilibrium, the end-members of the minerals are used to calculate an independent set of reactions where the equilibrium relationship can be expressed with the formula

$$0 = \Delta G^\circ + RT \ln K$$

Where ΔG° is a function of temperature and pressure, R is the gas constant, T is the temperature and K is the equilibrium constant, calculated from the activities of the end-members. The equilibrium relationship is a line in P-T space. Several independent reactions are combined with the least squares method to obtain the average P-T conditions of metamorphism (Powell and Holland 1994).

Before using THERMOCALC the mineral analyses in oxide percentage from the EMPA had to be recalculated to obtain the activities of the end-members. Tim Holland developed the software AX to recalculate oxides to a mineral formula and to calculate the activities of the end-members in the mineral. Many minerals occur as a solid solution of two or more end-members e.g. biotite has two main end members:

$KFe_3AlSi_3O_{10}(OH)_2$ - $KMg_3AlSi_3O_{10}(OH)_2$

annite - phlogopite

Thus biotite can have various proportions of these two end-members which will influence the reactivity of the mineral. The end-members activities can be proportional to its mole fraction. Higher mole fraction gives higher activity. For example a biotite from microprobe analysis with the following composition:

$$KFe_{0.6}\,Mg_{2.4}AlSi_3O_{10}(OH)_2$$

If this biotite has an ideal behavior the activity (a_{Fe}) of the end member annite will be the same as the mole fraction (X_{Fe}) of the end member:

$$a_{Fe} = X_{Fe}$$

In the above example the activity and the mole fractions of annite is 0.2. In general most minerals deviate from the ideal behavior and so do biotite therefore an activity coefficient (γ) is used to correct for non-ideal behavior:

$$a_{Fe} = \gamma_{Fe}\, X_{Fe}$$

The activity coefficient varies depending on pressure, temperature and composition. The activity coefficient is obtained from experimental studies and thermodynamic calculations.

Once the output file from AX is obtained with the end-members activities other pure phases present in the thin section e.g. H2O, SiO2 were added before running the file in THERMOCALC. With the information from the AX file, THERMOCALC calculates a number of independent reactions which are in turn used to constrain P and T.

Results

The study and sampling area is an approximately 10 km (west-east) and 20 km (north-south) wide (Fig 4). Most of the area is covered with moraine. However in the deformation zone there was good exposure of the bedrock. In total 41 samples were collected in 18 different localities. The samples were mainly of sedimentary and volcanic origin. To establish the metamorphic grade, metapelites and other metasediments with suitable mineral compositions were preferred for further investigations.

Petrographic study

In total 37 thin sections were studied; 25 thin-sections from the central part of the Nautanen Deformation Zone (NDZ), five from the west of the NDZ and seven from the east of the NDZ. Most samples were metapelites or other types of metasediments. However, from the central part of the NDZ, six samples were skarn and five samples andesite.

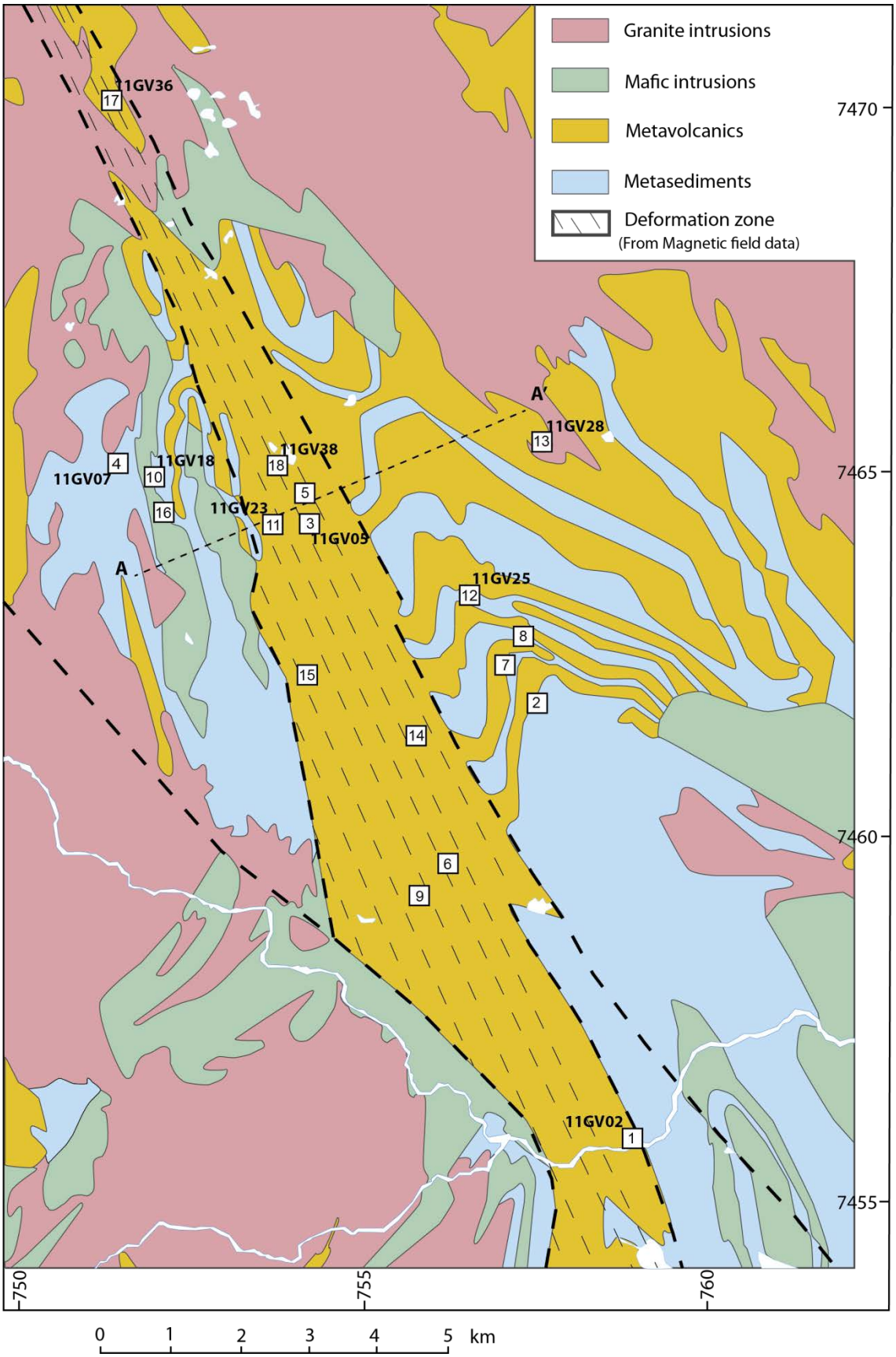

Fig. 4 Simplified bedrock map of the Nautanen area. Numbers in white squares mark sample localities. Sample discussed in the petrographic study is marked with sample number. The geochemical profile A-A' is indicated by the dotted line across the NDZ. Modified from SGU bedrock map Ai 100 (Witschard 1996).

On the west side there were two samples of altered diorite and from the east side two samples with andesitic origin. All thin sections were studied using a petrographic microscope and point counted. Variation in mineralogy and alteration was found in several thin-sections. In the discussion, I will show how these can be related to bulk composition, fluid infiltration and/or differing P-T conditions. The minerals found in thin sections of metasediments are listed in relationship to the NDZ in table 1. Garnet was found in 14 thin-sections within the NDZ but was not present outside the NDZ. Andalusite was found in three thin-sections east of the NDZ. The samples from the central part were more altered, showing replacement with sericite, epidote and/or chlorite. Because of these mineralogical differences, I have chosen to describe the sample in three groups: 1.West of the NDZ, 2. In the NDZ and 3. East of the NDZ.

Twelve thins section were selected for further investigation with the Scanning Electron Microscopy (SEM). Some of them were selected to analyse unknown minerals and some others were checked for suitability for further analysis by EMPA and if so, images were taken and analysis spots located. From the 12 thin sections, eight were selected for microprobe analysis. The mineral proportion for each of the thin-sections is found in table 2.

Mineral	Samples west of NDZ	Samples in NDZ	Samples east of NDZ
andaulsite	—	—	X
biotite	X	X	X
calcite	—	X	—
chlorite	—	X	X
cordierite	—	—	X
epidote	X	X	X
feldspar	X	X	X
garnet	—	X	—
muscovite	X	X	X
quartz	X	X	X
serecite	—	X	—
sillimanite	—	X	X
apatite	X	X	X
tourmaline	X	X	X

Table 1 Mineral distribution (metasediments) in relationship to the Nautanen Deformation Zone. Two samples in the northern part of NDZ close to the granite intrusion had sillimanite and garnet, all the other samples from NDZ had garnet as index mineral.

West of the NDZ

Samples from two different localities were described west of the NDZ (Fig. 4). Samples 11GV06 and 11GV07 were metapelites and the second sample 11GV18 was an altered diorite.

	West		In the NDZ					East	
Mineral	11GV07	11GV18	11GV23	11GV02	11GV05	11GV36	11GV38	11GV25	11GV28
amphibole	—	23,6	—	—	—	—	—	—	—
andalusite	—	—	—	—	—	—	—	4,3	6,6
biotite	2,0	19,9	60,2	14,2	—	17,5	1,9	11,9	41,2
calcite	—	4,5	—	0,7	0,3	—	—	—	—
chlorite	3,0	—	—	0,1	17,3	—	—	4,7	—
cordierite	—	—	—	—	—	—	—	2,7	—
epidote	3,4	—	6,5		24,8	—	—	—	—
feldspar	3,1	—	—	26,8	0,5	6,8	10,5	—	—
garnet	—	—	3,3	3,2	10,9	7,3	1,3	—	—
muscovite	38,8	—	16,3	3,8	—	7,0	33,8	16,9	2,8
opac	1,0	4,2	1,7	7,4	0,5	9,8	6,7	5,2	0,1
plagioclase	—	26,7	—	16,2	—	—	—	2,3	7,9
quartz	46,8	19,2	12,0	27,1	4,7	35,0	41,9	52,0	33,6
sericite	—	1,9	—	—	40,5	2,2	—	—	—
sillimanite	—	—	—	—	—	14,2	—	—	7,8
unknown	1,9	—	—	0,6	0,4	0,2	3,9	—	—
total	100,0	100,0	100,0	100,0	100,0	100,0	100,0	100,0	100,0

Table 2 The mineral proportion in % from the thin-sections described. The standard deviation range from ±0.1% - ±1.7% (van der Plas and Tobi 1965).

Locality 4 (67°11'44.50"N, 20°49'31.19"E)

Samples 11GV06 and 11GV07

These two samples are from the same outcrop and will be described together. The dominant rock type at the outcrop was quartzite but there was also some metapelite. There were a few large quartz veins with visible tourmaline crystals. The samples described were metapelites.

In thin section, the samples were fine grained with layers of aligned quartz, muscovite and some biotite and feldspar. Some of the muscovite crystals are not aligned parallel to the foliation. Secondary allanite-Ce crystals have grown on some of the muscovite (Fig. 5 and 6). The allanites were rimmed with epidote. Accessory minerals were tourmaline and apatite. Metamorphic allanite can form from igneous or detrital monazite by the reaction below (Gieré and Sorensen 2004).

monazite + biotite + plagioclase + quartz + fluid < -> apatite + allanite + muscovite

A few altered plagioclases were found in thin section (Fig. 5). All the minerals except monazite were found in the samples. If this reaction occurred, all the monazite must have been consumed. There was no evidence of relic monazite in the thin section. The metamorphic allanite could also have formed from a highly REE-rich fluid by hydrothermal reactions (Gieré and Sorensen 2004).
The chemical formula for the allanite-Ce mineral in the thin section calculated from microprobe analysis is $Ca(REE_{0.48}Ca_{0.46}Mn_{0.06})(Al_{2.09}Fe_{0.70}Mg_{0.18}Mn_{0.02})Si_{3.01}O_{12}(OH)$.

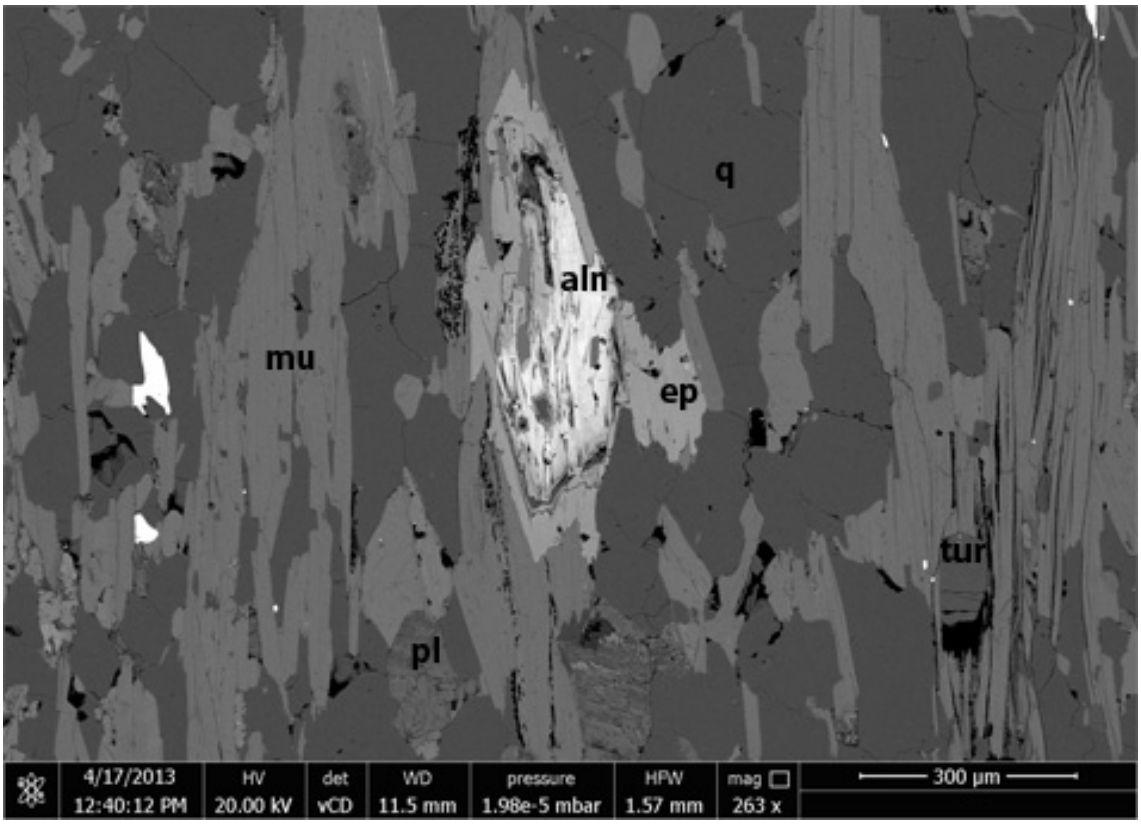

Fig. 5 Allanite (aln) rimmed by epidote (ep). Foliation defined by muscovite (mu) and quartz (q). Tourmaline (tur) and plagioclase (pl) crystals in the lower part of the image. Back-scattered image.

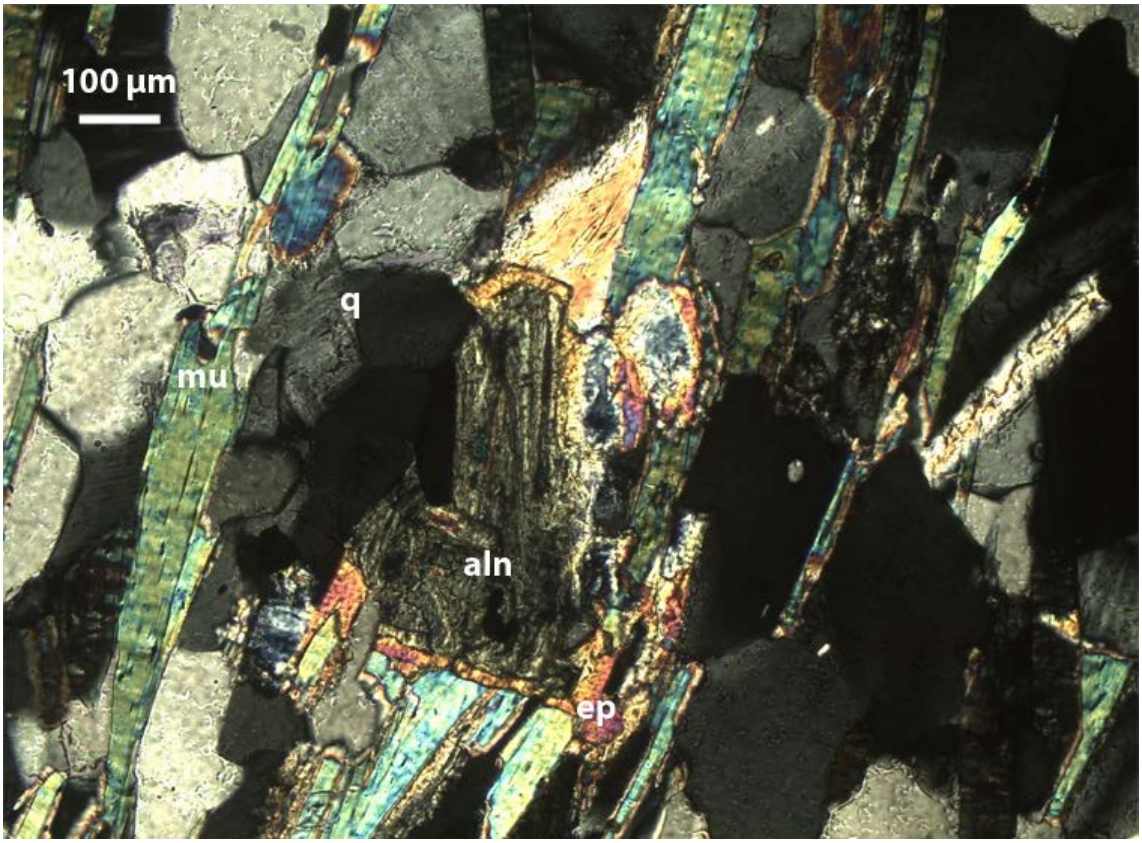

Fig. 6 Allanite (aln) rimmed by epidote (ep). Quartz (q) and muscovite (mu) define the foliation. Photomicrograph in cross polarized light (CPL).

Locality 10 (67°11'39.02"N, 20°50'2.49"E)

Samples 11GV18

The outcrop at this locality was the diorite intrusion. The rock was phaneritic.

The main minerals in the thin sections were plagioclase, amphibole, biotite and quartz. Biotite was replacing amphibole. Some of the plagioclase had some sericite in the center of the crystal. The accessories minerals were tourmaline and a lot of opaque minerals which were rimmed with calcite (Fig. 7). The calcite rim indicates that there have been reactions with a CO2 rich fluid.

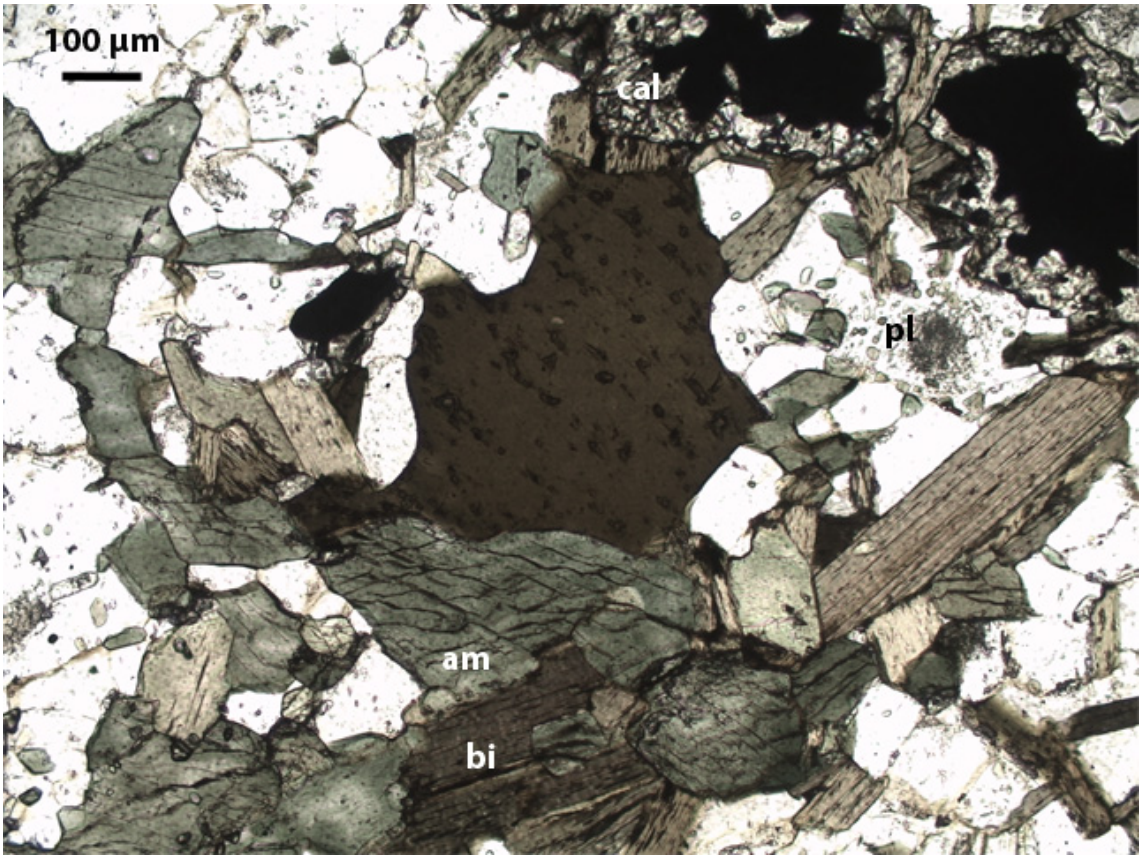

Fig. 7 Amphibole (am) being replaced by biotite (bi). Plagiocales (pl) some with sericite in the center and opaque minerals rimmed with calcite (cal). Photomicrograph in PPL

East of the NDZ

Two localities were studied east of the NDZ. The samples were 11GV25 and 11GV28 (Fig. 4).

Locality 12 (67°10'32.26"N, 20°56'30.43"E)

Sample 11GV25

At locality 12 the outcrop was metapelite with some compositional variations. There were a few quartz veins. Porphyroblasts of cordierite and/or andalusite were visible in hand specimen. In thin section fine grained biotite and quartz define a pervasive foliation. Cordierite porphyroblasts contained randomly orientated inclusions. The foliation wrapped around these porphyoblasts with strain caps and strain shadows (Fig. 8). This suggests that the cordierite was pre-tectonic. The andalusite porphyroblasts were syn- or post-tectonic and had overgrown the foliation (Fig. 8). Some randomly orientated chlorite crystals had partially replaced cordierite. These were post tectonic. There were two generations of opaque minerals; small elongated crystals in the foliation and larger euhedral crystals which were randomly orientated.

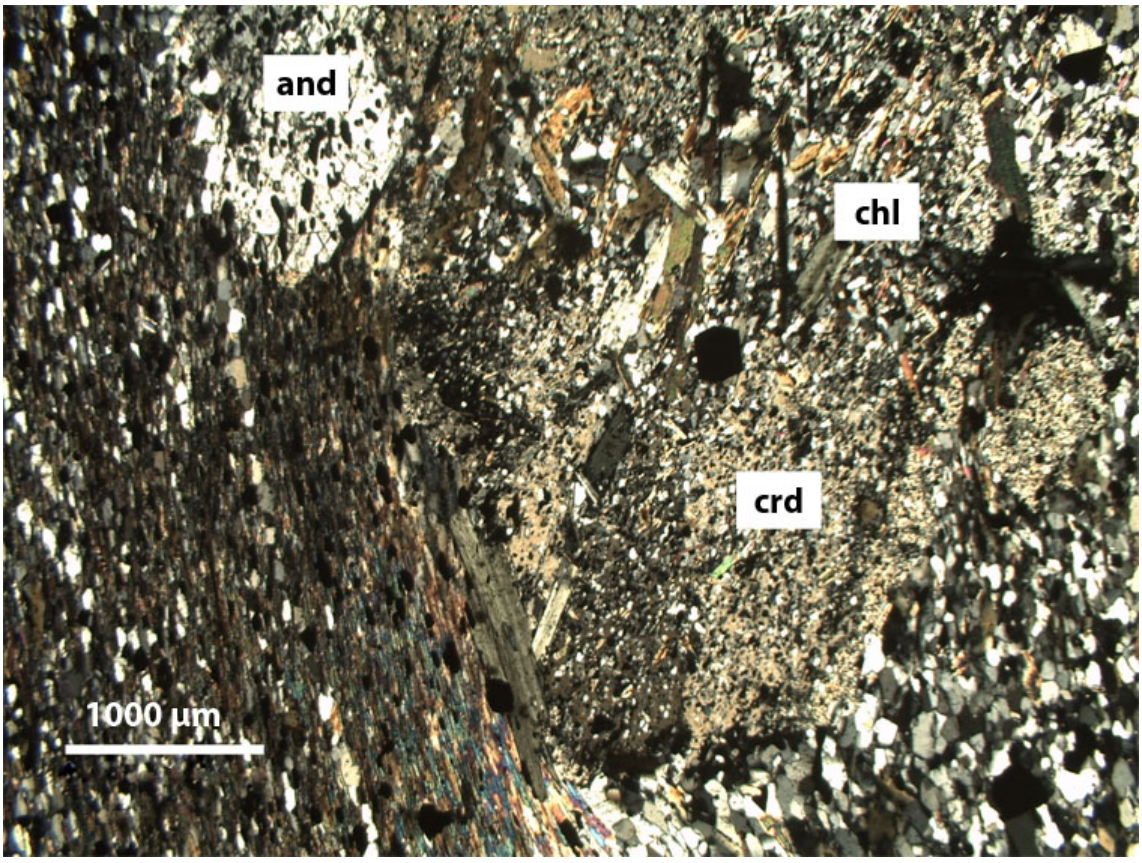

Fig. 8 Cordierite (crd) porphyroblast with strain cap to the left and strain shadow right bottom. Andalusite (and) porphyroblast has grown in the foliation. Chlorite (chl) is randomly orientated on the cordierite. Photomicrograph in CPL.

Locality 13 (67°11'43.19"N, 20°57'49.82"E)

Sample 11GV28

This was the most eastern locality and was close to the granite intrusion. The outcrop was mainly metapelite with some quartz veins. Porphyroblasts of andalusite were visible in hand specimen.

In thin section, the foliation was mainly defined by quartz, muscovite and biotite. There were andalusite porphyroblasts with large inclusions.

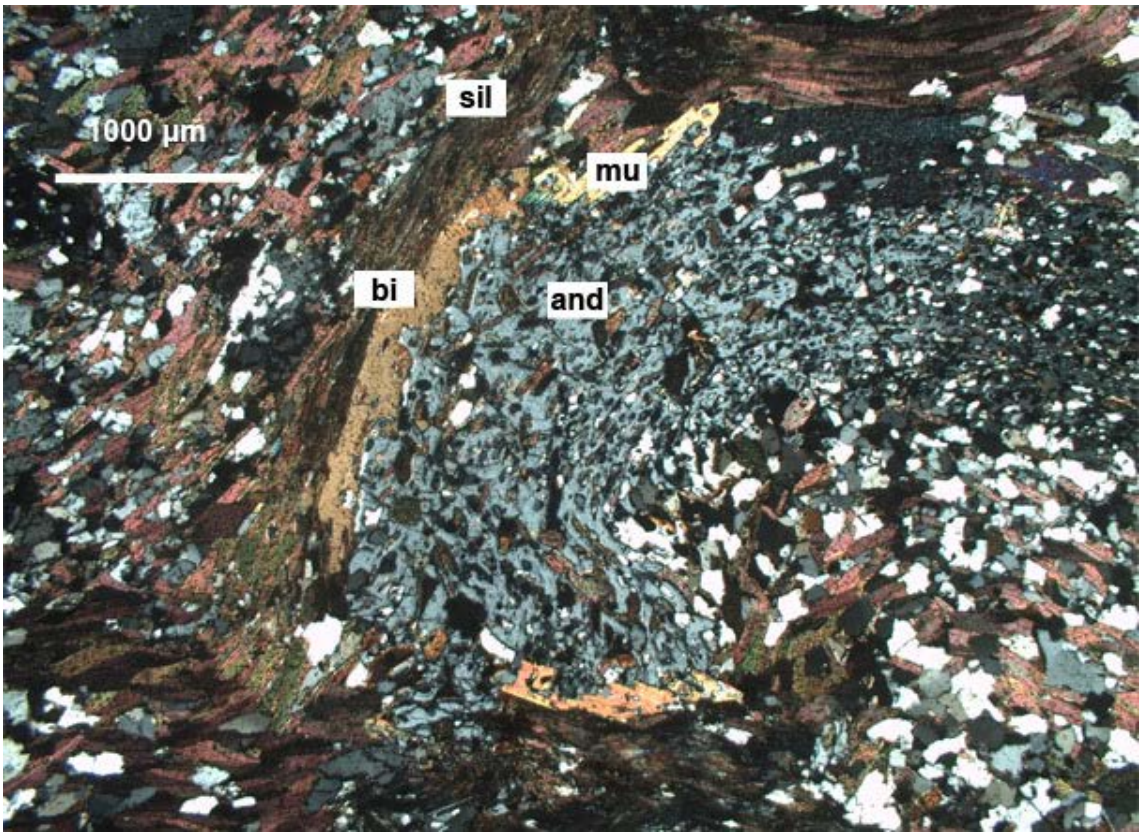

Fig. 9 Andalusite (and) rimmed by muscovite (mu), biotite (bi) and sillimanite (sil). Photomicrograph in CPL.

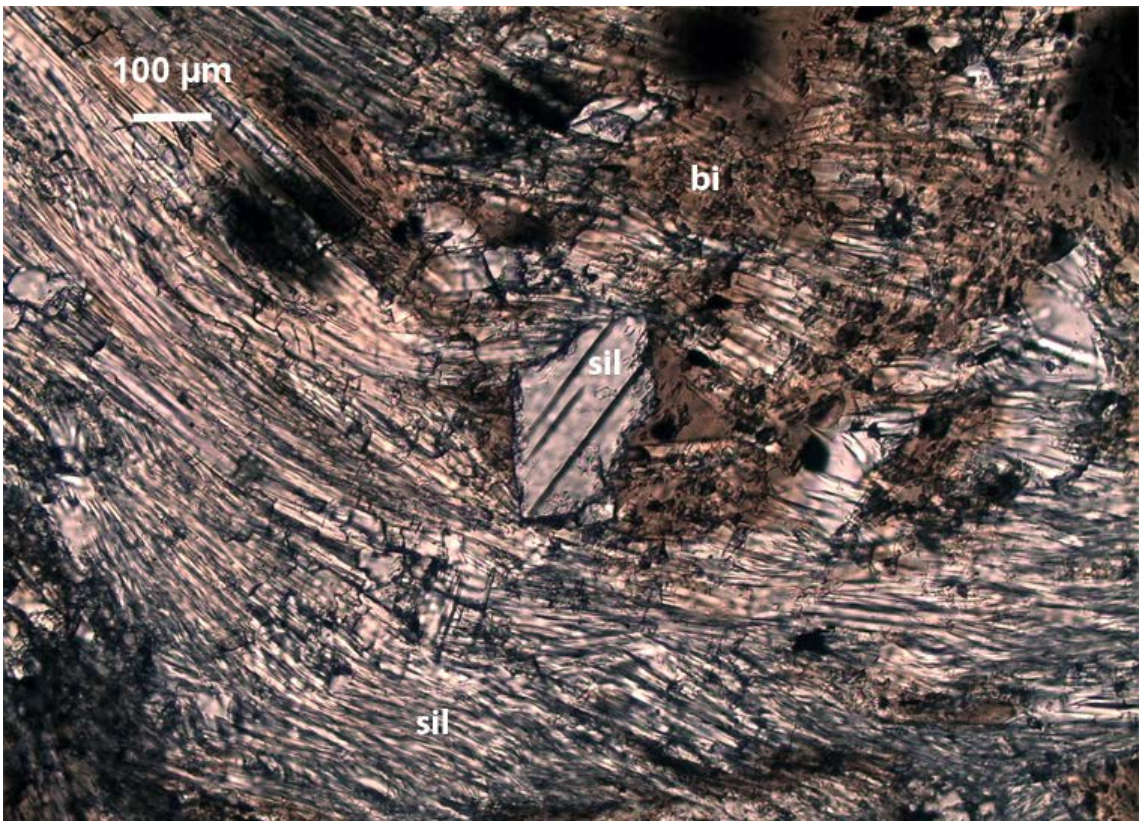

Fig. 10 A diamond-shaped sillimanite (sil) crystal with fibrous sillimanite (sil) and biotite (bi) in the matrix. CPL.

The inclusions in andalusite were consistent with the pervasive foliation. Andalusite was rimmed by muscovite, biotite and sillimanite (Fig 9). Some porphyroblasts of andalusite were replaced by muscovite, biotite and sillimanite. Diamond-shaped prismatic sillimanite crystals were also visible among fibrous sillimanite (Fig 10). SEM analysis detected an opaque mineral rich in Yttrium (40 wt%) and Phosphorus (33 wt%)which could be the mineral Xenotime-Y.

Central part of the NDZ

Samples 11GV36, 11GV38, 11GV23, 11GV05 and 11GV02 were situated in the central part of the NDZ. Garnet porphyroblasts were visible at most localities.

Locality 17 (67°14'52.97"N, 20°49'48.87"E)

Sample 11GV36

The locality was the northernmost and situated close to the granite intrusion. The outcrop was gneissic, and large garnet prophyroblasts were visible in hand specimen.

In thin section the matrix was strongly foliated and composed of elongated quartz, biotite, feldspar, opaque minerals and fibrous sillimanite. Garnet porphyroblasts were full of inclusions mainly quartz. Small veins cross-cut the foliation (Fig. 11).

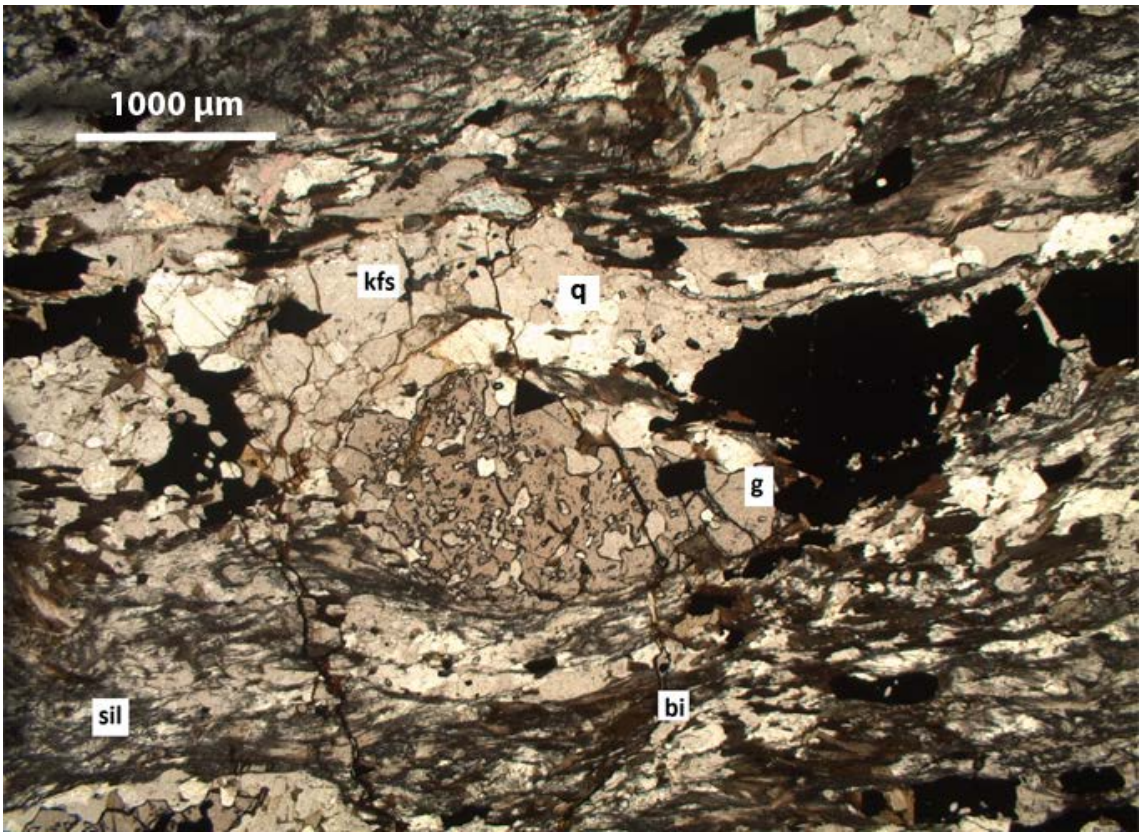

Fig. 11 Garnet (g) porphyroblast in a gneissic matrix with quartz (q), K-feldspar (kfs), sillimanite (sil) and biotite (bi). Photomicrograph in PPL.

A few muscovite crystals were visible but most of the muscovite had been replaced by K-feldspar.

SEM analysis detected high amounts of Sn at some spots on garnet (3-4 wt%). Microprobe analysis showed high concentration of Ba in feldspar (2.5 wt%) and in muscovite (0.7 wt%).

Locality 18 (67°11'37.89"N, 20°52'20.73"E)

Sample 11GV 38

The locality was close to an old copper mine in the NDZ (mine 29). There was a visible variation in composition at the outcrop. Some parts were rich in ore-minerals and/or biotite and some parts were richer in white micas. Garnet porphyroblasts were visible and occurred in various sizes, up to 15 mm Ø. The sample described here was schist metapelite.

In thin section the matrix was foliated and mainly composed of fine-grained quartz, muscovite, biotite and opaque minerals. There were some veins aligned parallel to the foliation. The core of the garnets was full of small inclusions whereas the rim had no inclusions.

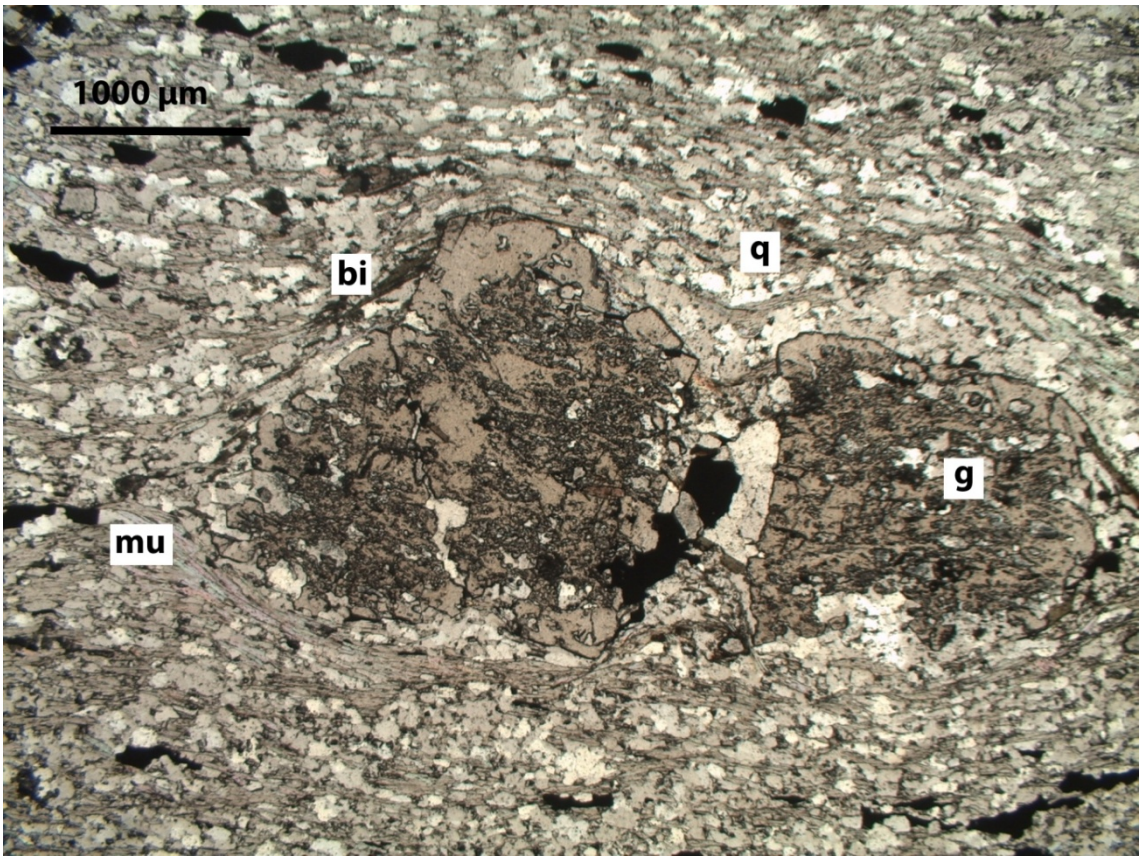

Fig. 12 Garnet (g) porphyroblast and matrix of muscovite (mu), quartz (q) and biotite (bi). Photomicrograph in PPL.

The actual foliation was deflected around the porphyroblasts with strain cap and pressure shadows (Fig 12). The garnets were partly replaced by opaque minerals and quartz in the

pressure shadow zone. In some garnets inclusion trails could be seen indicating an earlier foliation. These trails could not be traced into the pervasive foliation of the rock. They were randomly orientated, perhaps indicating some rotation of garnet crystals.

SEM revealed high concentration of Ba (2-3 wt%) in feldspar and spots with Sn in garnet (3 wt%).

Locality 11 (67°11'6.08"N, 20°52'54.07"E)

11GV23

This locality was also close to an old mine. The main rock type at the outcrop was biotite rich metapelite with a lot of garnet porphyroblasts. There was also skarn with epidote and garnet. The described thin-section was biotite rich metapelite.

In thin section, the matrix was seen to be mostly composed of biotite which defined a pervasive foliation. There was a large well shaped garnet in the thin-section. Secondary epidote and sericite patches had grown in the matrix (Fig 13). A compositional profile was constructed across a large garnet prophyroblast (Fig. 14 and 15), with spots measured every 9 µm. The steep shaped Mn profile may indicate garnet growth during prograde metamorphism and at greenschist facies conditions (Symmes and Ferry 1992).

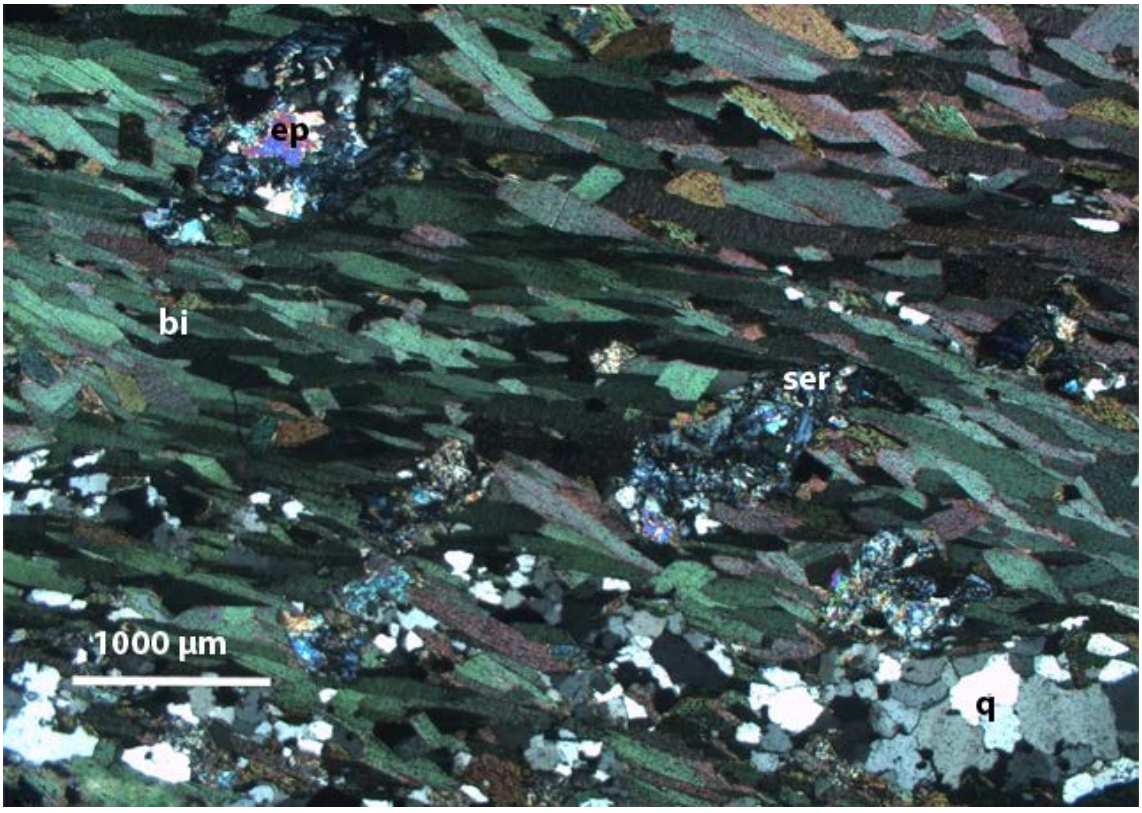

Fig. 13 Foliation defined by biotite (bi) and secondary sericite (ser) and epidote (ep). Some quartz (q) in the lower part of the picture. Photomicrograph in CPL.

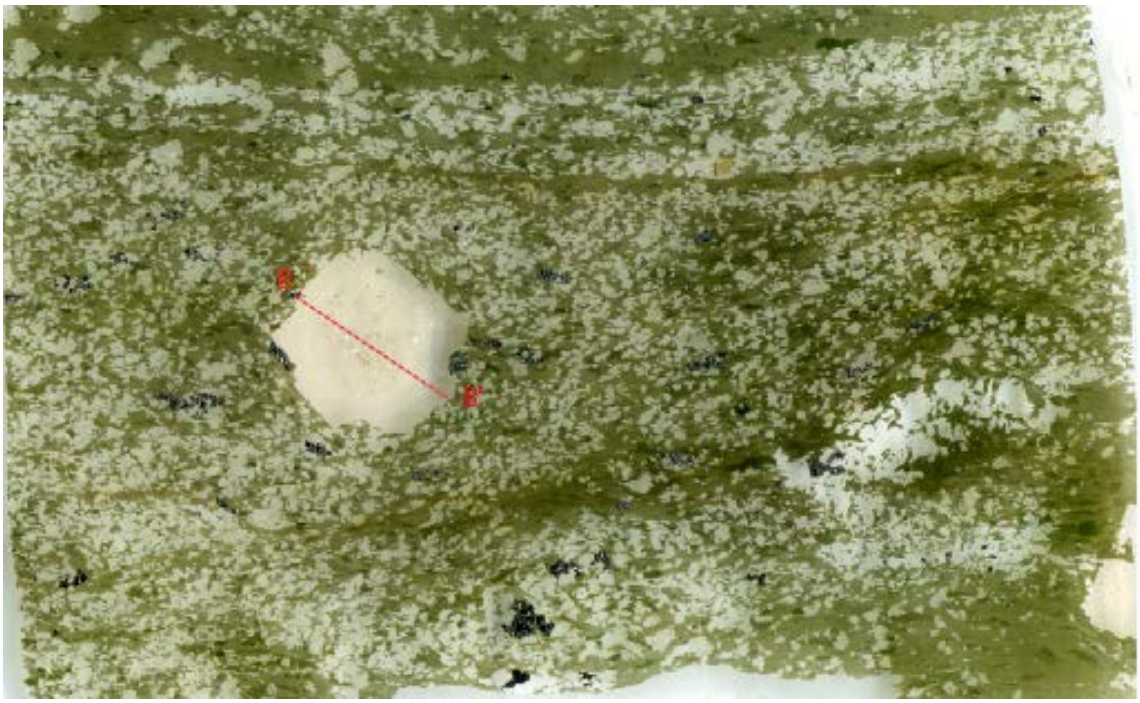

Fig. 14 A compositional profile B-B' was constructed across the large garnet porphyroblast in thin section 11GV23.

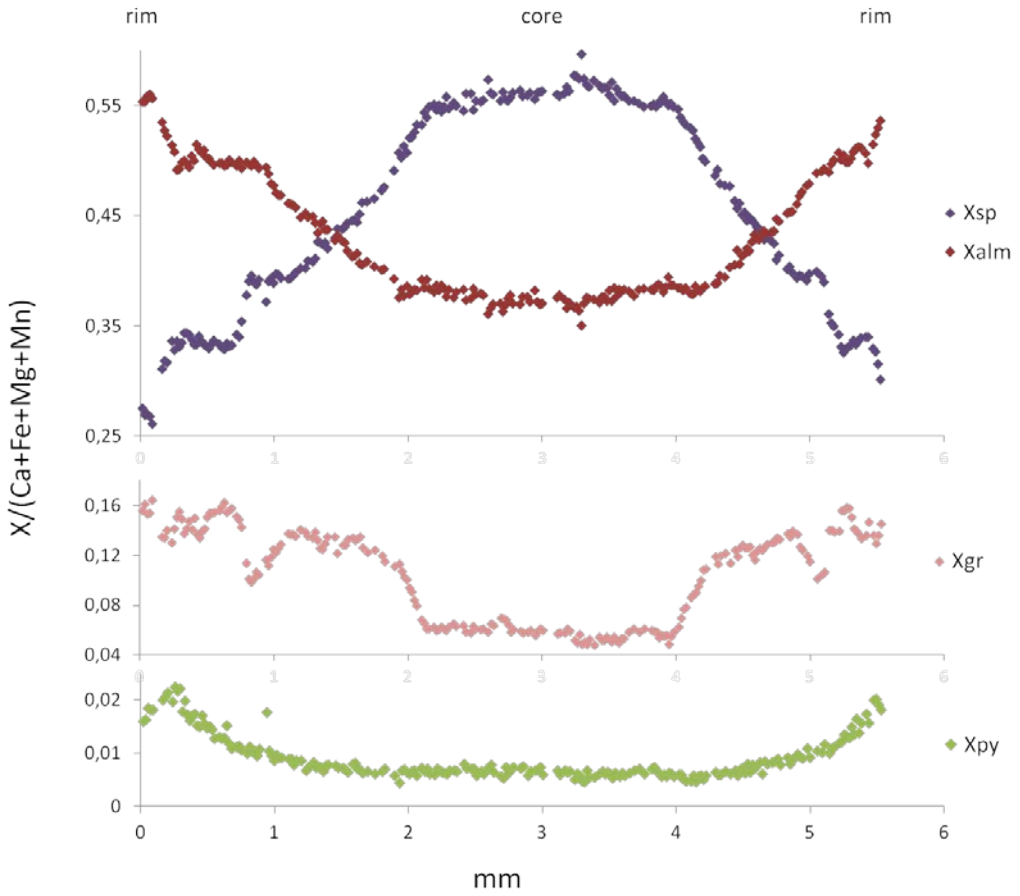

Fig. 15 Zoned garnet profile from the thin section shown in fig. 14. Proportion of spessartine, almandine, grossular and pyrope traverse the profile.

Locality 3 (67°11'4.16"N, 20°53'12.84"E)

11GV05

The outcrop at locality 3 was 250 m east of locality 11. The outcrop was skarn with visible layers of epidote, red- layers of feldspar and abundant small garnets.

In thin section, the matrix was seen to be altered and composed of sericite, chlorite, feldspar and epidote crystals. The matrix was foliated. The majority of the garnet porphyroblasts had been replaced by chlorite (Fig. 16).

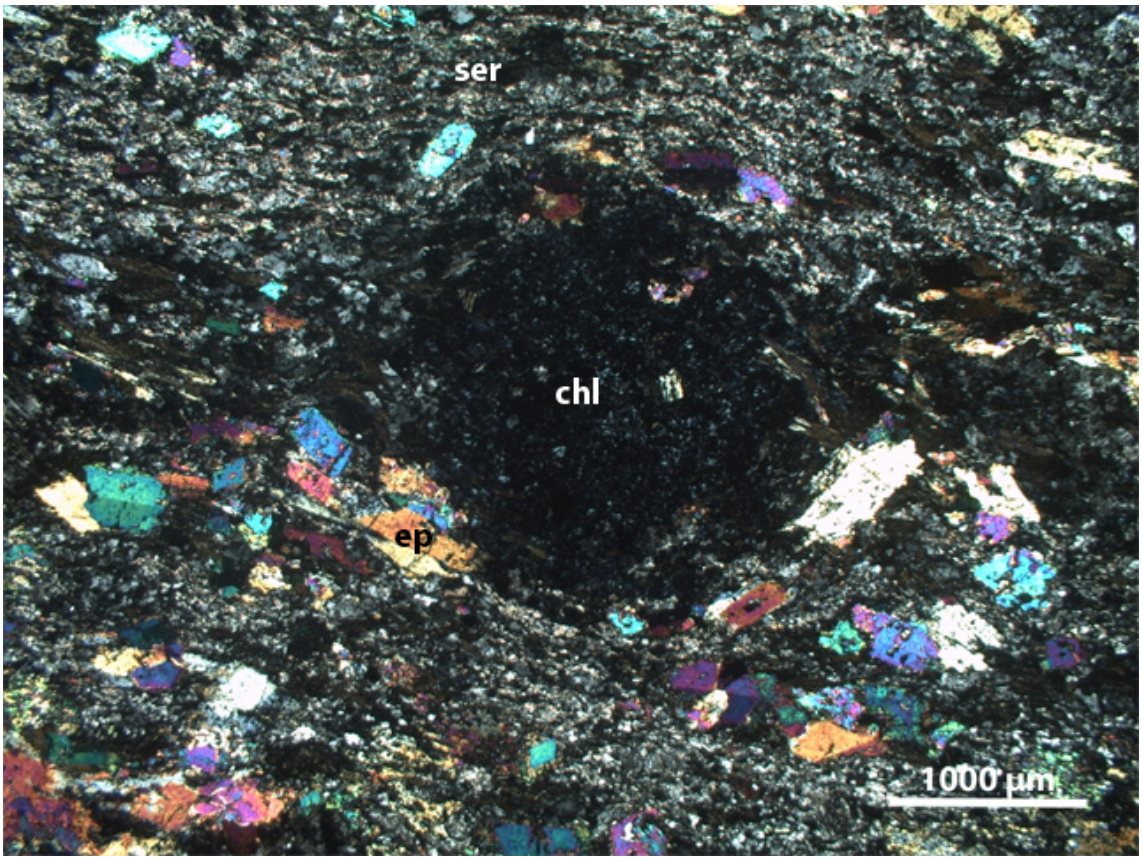

Fig. 16 Garnet is replaced by chlorite (chl) and the matrix is serecite (ser) and secondary epidote (ep) crystals. Photomicrograph in CPL.

Locality 1 (67° 6'28.06"N, 20°58'25.51"E)

11GV02

This is the southernmost locality which is situated close to the River Lina. The sample was a metapelite with visible garnet in hadspecimen.

In thin section, the garnet porphyroblasts were altered and partly replaced by chlorite and quartz. There were some quartz veins. The matrix was fine-grained, foliated and contained

quartz, K-feldspar, plagioclase, muscovite and opaque minerals. In some parts, the matrix was altered to sericite. The foliation defined by muscovite was crenulated (Fig. 17).

The microprobe analysis gave very high Mn content in garnet; 25-26 wt%, in both core and rim spot analyses. SEM detected high levels of Sn at some spots in garnet (4 wt%).

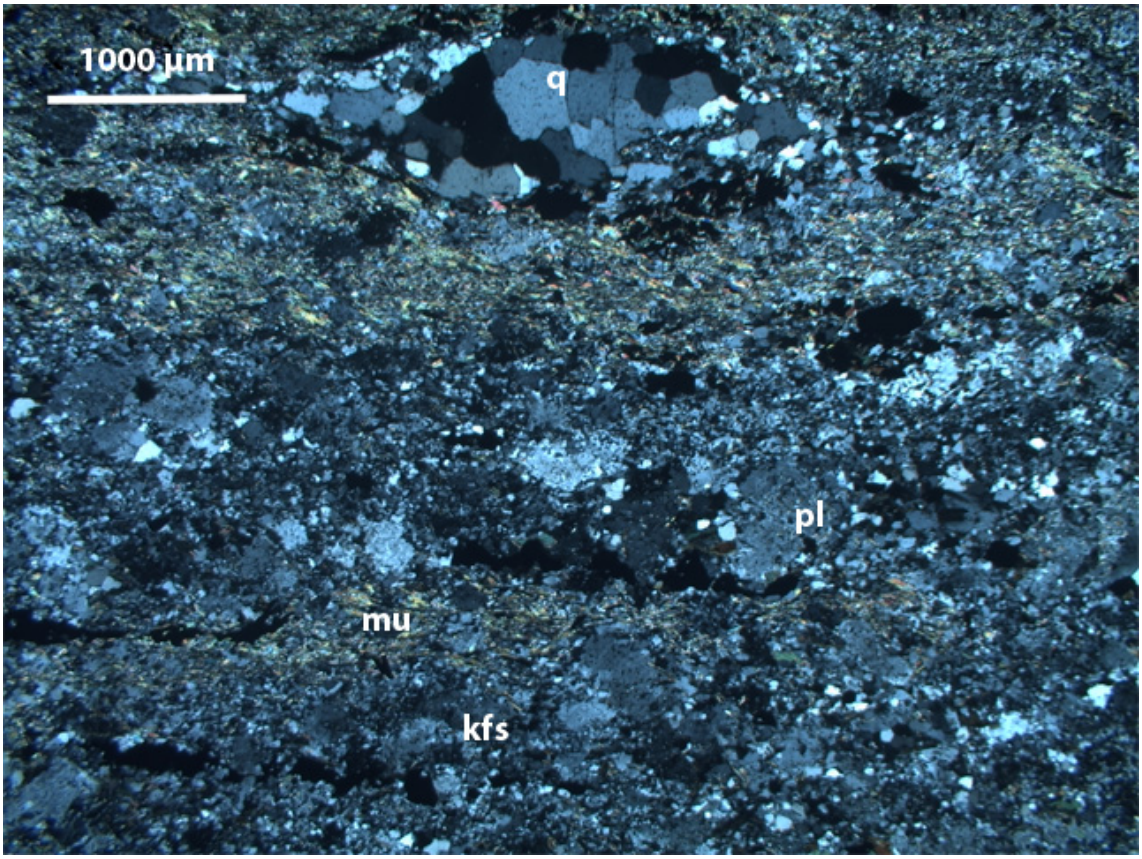

Fig. 17 Porphyroblast replaced by quatz (q) and altered matrix with muscovite (mu), K-feldspar (kfs) and plagioclase (pl). The foliation defined by muscovite was crenulated. Photomicrograph in CPL.

Geochemical results

Out of the 40 samples, 21 were selected for XRF analysis. The protolith was sediment for 18 of these samples and andesite for three samples. The major elements in oxides; SiO2, Al2O3, CaO, Na2O, K2O, Fe2O3, MgO, MnO, TiO2, P2O5 and some trace elements were analysed.

To compare the concentration of trace elements, a spider diagram was used. The trace elements used were large ion lithophiles (LIL) elements; Sr, K, Rb and Ba which were plotted on the left side of the diagram and high field strength (HFS) elements; Th, Nb, Ce, P, Zr, Hf, Ti and Y which were plotted on the right side. The samples were normalized to the North American shale composite (NASC) which represent average crustal material (sediments and metasediments) from different continents (Condie 1993). NASC were chosen as the majority of the analysed samples were metapelites and NASC makes a good reference for pelites before metasomatism. In Fig. 18 most elements from the samples were similar to NASC, what stands out was that several samples had high concentrations of Ba.

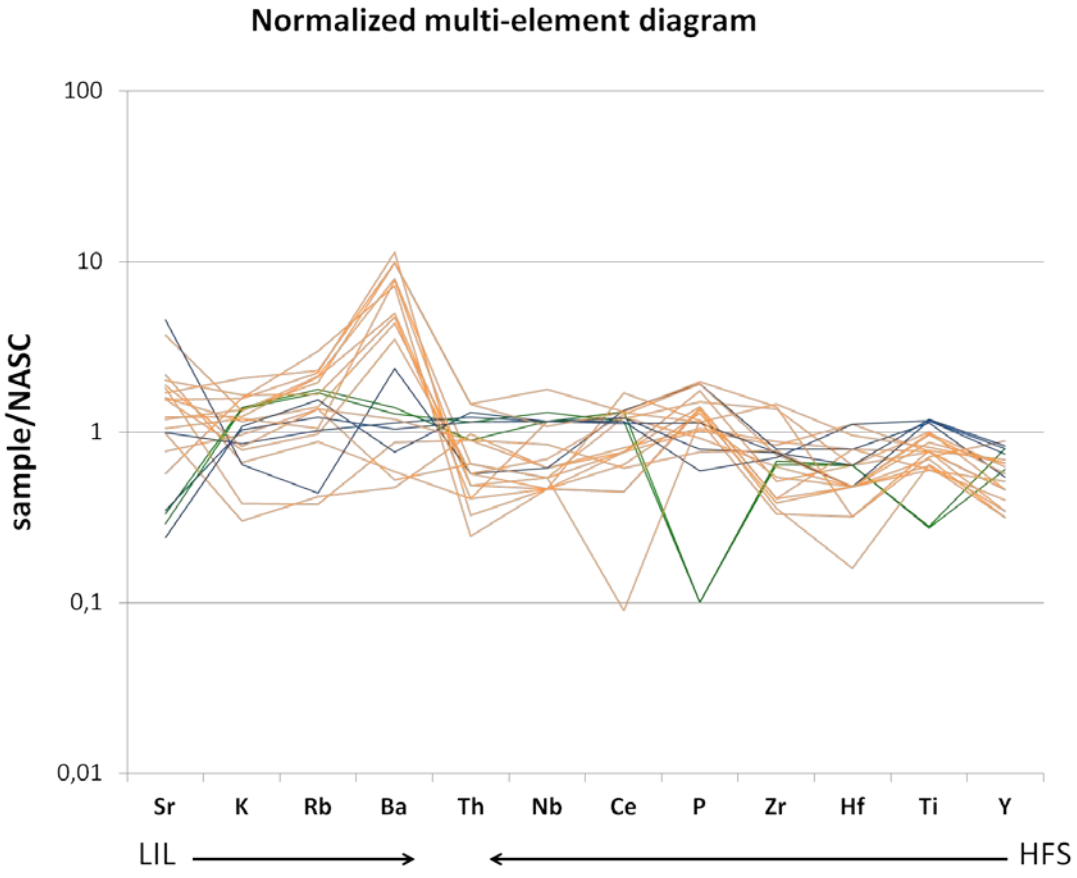

Fig. 18 Multi-element diagram normalized to NASC (Condie 1993).. The orange lines show samples from the NDZ, the blue lines from east of the NDZ and the green lines from west of the NDZ. The arrows indicate the direction for higher mobility of the elements.

One sample 11GV38 had negative Ce anomaly this was probably due to error in analysis or preparation. Two samples from the west side of the NDZ (11GV06 and 11GV07) had negative P anomalies.

The concentration of Ba in the bulk composition was high. It was between 2000 to 7000 ppm in 11 of 20 samples. The Ba concentration was plotted along a 5.5 km profile from west to east and perpendicular to the deformations zone (Fig. 4). The high concentrations of Ba were located in or close to the NDZ (Fig. 19).

The major elements in oxides were also plotted across the 5.5 km profile (Fig 20). The three samples of meta andesite had high Na2O concentrations (5 - 6 wt. %). The samples from the NDZ had higher concentrations of MnO and Fe2O3. The two samples (11GV07, 11GV06) from the western part had low TiO2 (Fig. 20).

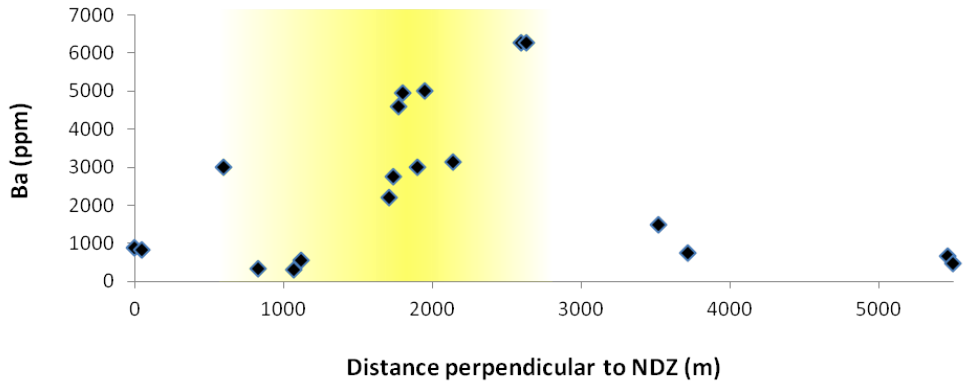

Fig. 19 Barium concentrations in ppm across the profile A-A' from Fig. 4. The yellow colour indicates the deformation zone.

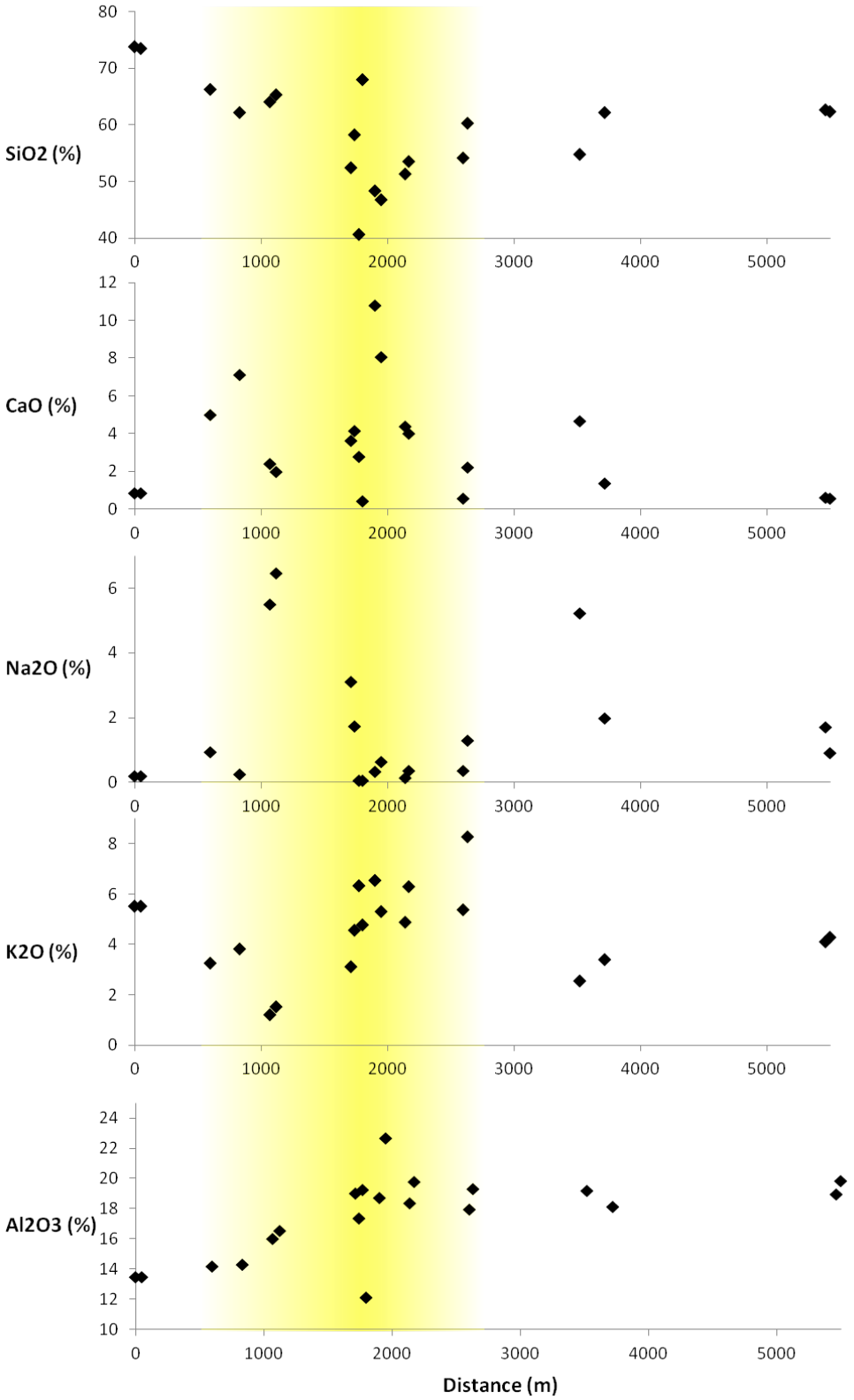
SiO2 (%)
80
70
60
50
40
0
1000
2000
3000
4000
5000
CaO (%)
12
10
8
6
4
2
0
Na2O (%)
K2O (%)
Al2O3 (%)
24
22
20
18
16
14
12
10
Distance (m)

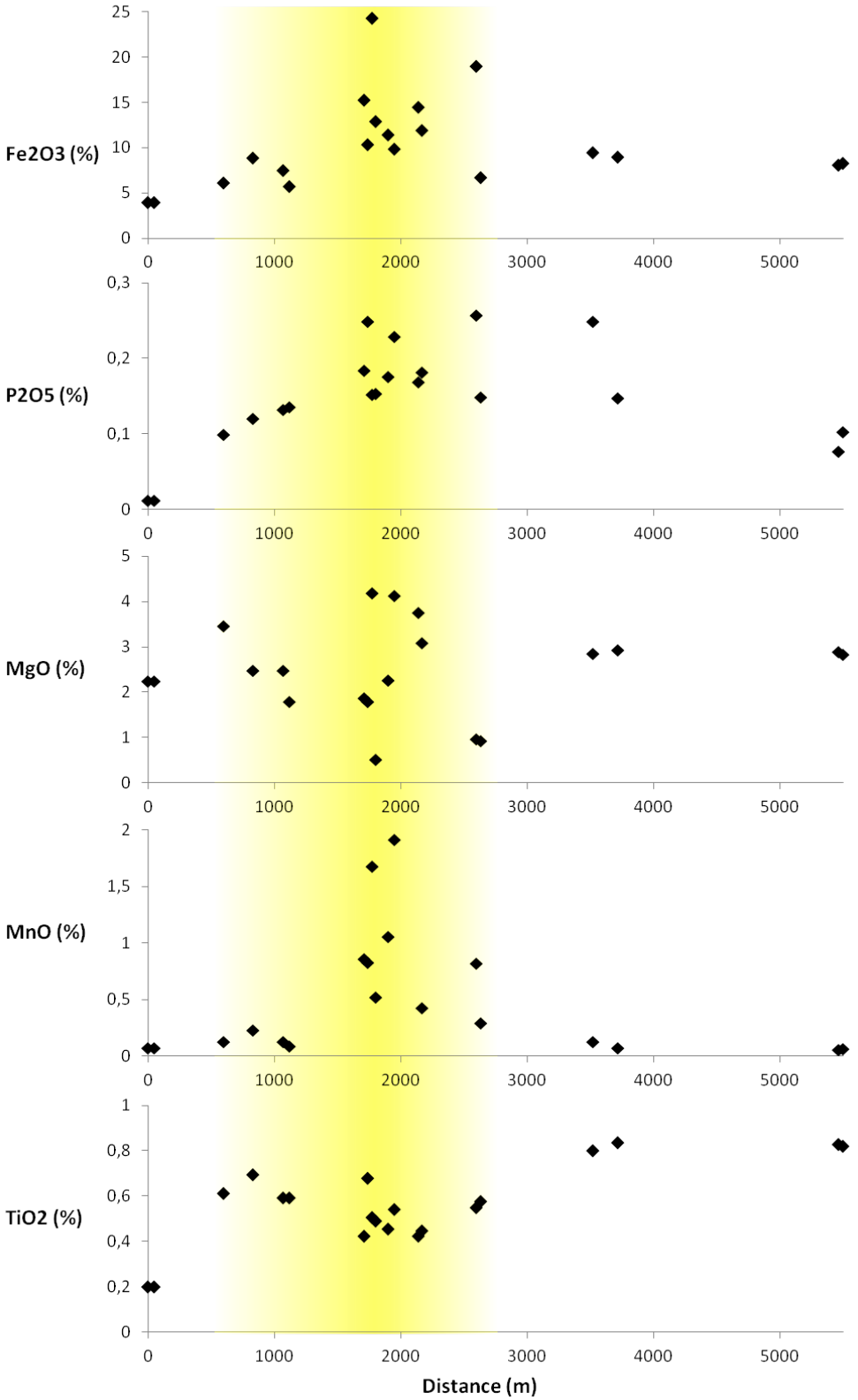

Fig. 20 Major elements in oxides from analysed samples along the A-A' profile from Fig. 4. The yellow colour indicates the NDZ.

Results from THERMOCALC

To calculate average PT for metamorphism with THERMOCALC, it is useful to have reactions which are good thermometers and good barometers. I first tried to calculate P and T simultaneously for all the samples. For samples 11GV25, 11GV28, 11GV36 and 11GV38, an independent set of reactions was calculated and reasonable average P-T estimates were obtained (Tab. 3). For the four other samples, there were too few reactions to calculate average P and T. For these samples it was, however, possible to calculate average T for a predefined fixed pressure. Sample 11GV02 did not give any results probably due to disequilibrium, so it was excluded. The four remaining samples had too few reactions and/or no good barometers to obtain results for average P. From the petrographic study I could assume that the pressure should be in the andalusite stability field for sample 11GV25 and 11GV28. The average pressure obtained from samples 11GV36 and 11GV38 confirmed this assumption for the NDZ even though andalusite was not present in these samples. Average T was calculated for a pressure set to 3 kbar for samples 11GV23 and 11GV07. This pressure was close to that which was obtained from samples for which both P and T could be calculated (Tab. 3). Samples 11GV05 only gave a result for average T at pressure 3.5 kbar. The sigmafit for 11GV05 was above what is recommended by THERMOCALC, but as the other diagnostic information was acceptable the result has been included. In table 3 the results are listed with the activities of the end members calculated with AX, the added phases, the number of reactions and the excluded end members. Standard deviation for P and T are listed and two diagnostic values on the data performed by THERMOCALC:

1. Correlation coefficient indicates the degree to which the end member reactions are correlated. This highlights how strongly uncertainties influence calculated values of P and/or T. Zero means uncorrelated reactions and one means perfectly correlated reactions.

2. Sigmafit (fit) is a test run by the program on the confidence of the data. The sigmafit should ideally not be larger than 1.0. However it can exceed 1.0 depending on the input data, the maximum recommended sigmafit is calculated by the program and printed (Powell and Holland 1994).

The results from THERMOCALC average PT and the average T with error bars were plotted in the PT- space (Fig. 21).

The complete THERMOCALC files for the calculated samples can be found in the Appendix C.

Sample	**11GV38**	**11GV36**	**11GV28**	**11GV25**	**11GV23**	**11GV07**	**11GV05**
P-T stage	prograde	prograde	prograde	prograde	retrograde		retrograde
Activities at	600˚C	660˚C	700˚C	550˚C	500˚C	600˚C	500˚C
Garnet	rim	rim			rim		rim
py	0,00017	0,00042	—	—	0,00023	—	0,00019
gr	0,0005	0,00016	—	—	0,0112	—	0,021
alm	0,089	0,29	—	—	0,11	—	0,0063
spss	0,07	0,0087	—	—	0,014	—	0,09
andr	—	—	—	—	—	—	0,0605
Biotite							
phl	0,0223	0,0167	0,03	0,126	0,0111	0,35	—
ann	0,099	0,095	0,06	0,0087	0,085	0,0013	—
east	0,02	0,2	0,007	0,111	0,02	0,18	—
Muscovite							
mu	0,63	0,7	0,79	0,75	0,79	0,57	—
cel	0,0104	0,0094	0,0091	—	—	0,021	—
fcel	0,019	0,008	0,008	—	—	0,0123	—
pa	0,087	0,0184	0,202	—	0,077	0,054	—
Plagioclase							
an	—	—	0,23	0,42	—	—	—
ab	—	—	0,85	0,75	—	—	—
Chlorite							
clin	—	—	—	0,132	—	—	0,12
daph	—	—	—	0,00172		—	0,0028
ames	—	—	—	0,13	—	—	0,0586
Alkali feldspar							
san	0,93	0,88	—	—	—	0,96	0,94
ab	0,378	0,51	—	—	—	0,211	0,548
Cordierite	—	—	—	—	—	—	—
crd	—	—	—	0,69	—	—	—
fcrd	—	—	—	0,0062	—	—	—
mncrd	—	—	—	0,00024	—	—	—
Epidote							
cz	—	—	—	—	0,85	0,32	0,21
ep	—	—	—	—	0,15	0,62	0,73
Other	q H2O	q H2O sil	q H2O and sil	q H2O and	q H2O	q H2O	q H2O
Results							
aH2O	1	1	1	1	1	1	1
T˚C	**620**	**668**	**681**	**589**	**510**	**584**	**474**
s.d (T)	39	40	14	41	61	32	43
P kbar	**4**	**3,3**	**2,5**	**4,3**	**3**	**3**	**3,5**
s.d (P)	2,6	1,3	0,2	1,5			
correlation	0,855	0,962	0,474	0,989			
fit	0,29	0,93	0,7	1,4	0,8	1	2,2
nr of reactions	5	6	5	7	3	4	4
excluded	fcel	fcel		fcel, cel		ep, cz	san, ab

Tab. 3 Average PT and average T calculated for seven samples with THERMOCLAC 3.33. Endmember abrevations and names can be found in Appendix A.

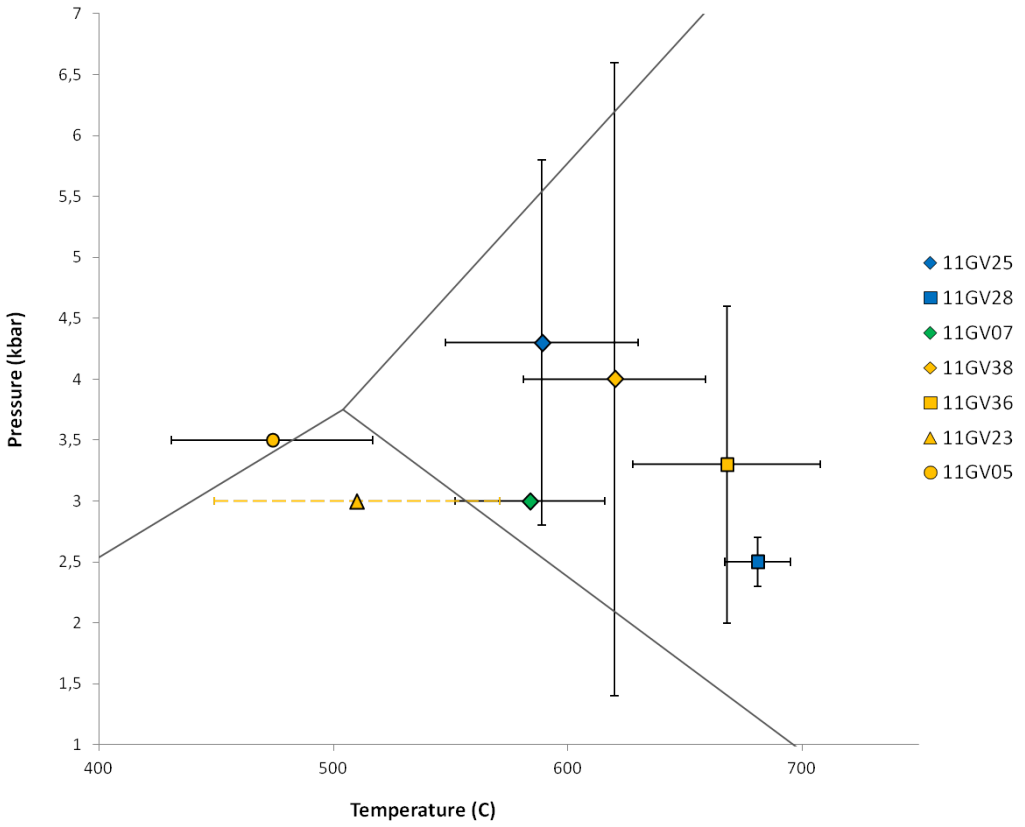

Fig. 21 Average PT plotted in the PT-space with error bars. Sample 11GV23 has orange dotted error bars for visibility. The icons for samples from NDZ are orange, east of NDZ blue and west of NDZ green. The aluminium silicate stability diagram is from Holdaway et al. 1993.

Discussion

In this section I will first discuss the metamorphic grade indicated by the mineralogy in thin section. Thereafter the results of P-T modelling using THERMOCALC and the geochemical results will be discussed.

Petrology

Two samples from outside the NDZ contain prophyroblasts of andalusite. These are samples 11GV25 and 11GV28 (Fig. 4). Sample 11GV25 also contains cordierite porphyroblasts (Fig. 8), and sample 11GV28 contained no cordierite but sillimanite (Fig. 9 and 10). These two samples were both metasediments and of similar bulk compositions (Appendix B). These mineral occurrences will be discussed here.

In sample 11GV25, the cordierite porphyroblasts were full of inclusions, which were randomly orientated. The foliation was wrapped around the cordierite with strain caps and pressure shadows. In contrast, andalusite prophyroblasts overgrow the same foliation. This indicates sequential growth of cordierite and andalusite. Cordierite grew before deformation, indicated by the randomly orientated inclusions and by the fact that the pervasive foliation wraps around the cordierite crystals. Andalusite grew after deformation, overgrowing the pervasive foliation. Finally, retrograde randomly oriented crystals of chlorite grew, replacing cordierite. Sequential growth of cordierite and andalusite has been described by R.H. Vernon (1988) with the following reaction:

cordierite + muscovite <-> andalusite + biotite + quartz

In sample 11GV28, the andalusite porphyroblasts contain inclusions that are aligned parallel to the pervasive foliation. The andalusites had reaction rims of muscovite, biotite and sillimanite. These micas are not clearly aligned with the foliation: some follow the foliation and some are randomly orientated. There are also a few andalusite crystals that are partly replaced by randomly orientated muscovite.

From the mineral relationships in these two samples, I suggest three metamorphic events: One regional metamorphic event indicated by sequential growth of cordierite and andalusite; a second stage also affecting both samples with retrograde growth of randomly orientated chlorite replacing cordierite and randomly orientated muscovite replacing andalusite; and a third stage of contact metamorphism affecting only sample 11GV28 and recorded by the replacement of andalusite by sillimanite.

In the NDZ, two metapelite samples can be compared in a similar way. These are samples 11GV38 and 11GV36 (Fig. 4). Sample 11GV38 contains garnet porphyroblasts and a fine grained foliated matrix of quartz, micas and opaque minerals (Fig. 12). The matrix is deflected around the garnet. Some of the garnets contain small inclusions in the core indicating an earlier foliation. This foliation cannot be traced into the pervasive foliation of the rock. The garnet rims are inclusion poor. Sample 11GV36 contains garnet porphyroblasts, and a strongly foliated gneissic matrix with elongated quartz, biotite, K-feldspar and fibrous sillimanite (Fig. 11). There are a few muscovite crystals with reaction rims. The interpretation of these relationships is an earlier deformation event indicated by the inclusions in some of the garnets. The garnets were syn- or post-tectonic with respect to this first deformation event. A second deformation event is interpreted from the foliation that is deflected around the garnet porphyroblasts. In sample 11GV38 some garnets have been partly replaced by quartz in the pressure shadows. Only sample 11GV36 was affected by contact metamorphism which is demonstrated by muscovite replaced by k-feldspar and the appearance of fibrous sillimanite. It is possible that the second deformation event and the contact metamorphism were simultaneous or close in time. A compositional profile was constructed along a garnet porphyroblast from the NDZ (Fig. 14 and 15). The garnet was extremely Mn-rich. The core was composed of 55% spessartine and 35% almandine. At 20 mm from the rim the Mn content drops steeply and the Fe content increases. At the rim the spessartine content was 25% and almandine content was 55%. This type of profile suggests growth during prograde

metamorphism. Mn preferentially goes into garnet and stabilizes the mineral at lower temperature, e.g. greenschist facies (Symmes and Ferry 1992). This garnet profile is consistent with a regional metamorphic event affecting the NDZ. The profile also shows reversed zoning near the garnet rims which match the later retrograde event described in the following samples from the NDZ.

All the other samples (11GV23, 11GV05 and 11GV02) from the NDZ show evidence of retrogression, such as retrograde growth of sericite, chlorite and epidote. In sample 11GV05 the garnet porphyroblasts are replaced by chlorite. These retrograde reactions have partly overprinted evidence of earlier prograde metamorphic reactions and thus indicate late stage fluid mobility.

On the west side of the NDZ, three samples were described (Fig. 4). Sample 11GV18 was an altered diorite which shows evidence of having been altered by reaction with a CO2-bearing fluid (Fig. 7). The second and third samples 11GV06 and 11GV07 were quartz rich metapelites with metamorphic allanite (Fig. 5 and 6). The samples were close to both the granite intrusion and the diorite intrusion (Fig. 4). Several studies have focused on metamorphic allanite and its phase relations with monazite from low-grade metamorphism up to amphibolites facies (Ferry 2000; Boswell et al. 2002; Gieré and Sorensen 2004; Janots et al. 2008). Metamorphic allanite can form from detrital or igneous monazite. A possible reaction for the formation of allanite from Gieré and Sorensens (2004) is:

monazite + biotite + pagioclase + quartz + fluid -> apatite + allanite + muscovite

In samples 11GV06 and 11GV07, all these minerals were present except monazite. The monazite could have been consumed.

Janots et al. (2008) demonstrate that monazite reacts to form allanite, and that monazite is consumed and disappears above c. 450˚C. Depending on the bulk CaO/Na2O ratio of the rock, allanite can be stable at temperatures up to 600-610˚C. These high grade allanites tend to be rimmed with epidote (Janots et al. 2008). If this applies to samples 11GV06 and 11GV07, where metamorphic allanite was present, rimmed with epidote, and with high CaO/Na2O ratio in the bulk composition, then it is consistent with the relatively high metamorphic grade evaluated for sample 11GV07 (Tab. 3). From the mineral and texture relationship in samples 11GV06 and 11GV07, I suggest a first metamorphic event indicated by the foliation of muscovite, biotite and quartz. A second contact metamorphic event related to one of the two intrusions indicated by the growth of metamorphic allanite. For this reaction the presence of a fluid is needed. This fluid could have its origin from the diorite intrusion or the granite intrusion. This hypothesis is tentative and requires further investigation e.g. with more samples from this part of the study area. It would also be interesting to date the allanites because this might allow for the age of the metamorphic event to be constrained.

In summary, two samples (11GV28 and 11GV36) and possibly also 11GV07 show evidence of contact metamorphism. In samples 11GV28 and 11GV36, contact metamorphism has partly overprinted an earlier metamorphic event. The earlier metamorphic event was visible in

samples 11GV25, 11GV38 and in the garnet profile from sample 11GV23. Several samples (11GV23, 11GV05 and 11GV02) from the NDZ show evidence of retrograde reactions.

The metamorphic grades interpreted from mineral reactions in thin sections are in agreement with Bergman et al. (2001) for samples collected from the NDZ. All the samples from the NDZ show evidence of medium grade metamorphism with the exception of sample 11GV36 which shows evidence of higher metamorphic grades documented by the occurrence of sillimanite and K-feldspar. However, in contrast to Bergman et al. (2001), evidence from this study suggests that some samples from outside the NDZ were also metamorphosed at medium grade conditions. Evidence of high grade metamorphism was restricted to one sample close to the granite intrusion. In further research it would be interesting to extend the profile towards the east and the west to investigate a change in metamorphic grade.

THERMOCALC

The temperatures obtained from THERMOCALC are mostly in agreement with the petrographic evidence for metamorphic grade discussed above. In Fig. 21, three metamorphic events can be distinguished in the plotted temperature and pressure:

1. Samples 11GV25 and 11GV38 show evidence of an earlier regional metamorphic event in thin sections. The calculated pressure and temperature from these two samples are in agreement with each other. The standard deviation for the pressure is relatively high for both samples. I infer that these results represent the peak metamorphic T and P for the regional metamorphic event that affected the Nautanen area. However in sample 11GV25, andalusite rather than sillimanite was present; therefore the calculated peak pressure for this sample is too high as the sample plots in the sillimanite field (Fig. 21). However the standard deviation for pressure was large suggesting that pressure was constrained on the basis of too few reactions.

2. The two samples 11GV36 and 11GV28 were both close to the granite intrusion. The averages PT are consistent with a contact metamorphic event. Sample 11GV07 was also close to intrusions but it was not possible to calculate average P. As discussed above in the petrology section, further investigations are needed to confirm the metamorphic history of this locality.

3. Three samples from NDZ showed evidence of retrogression: 11GV23, 11GV05 and 11GV02. It was not possible to calculate average PT for any of these samples. The pressure was assumed to be 3 kbar. With the fixed pressure of 3 kbar, respectively 3.5 kbar (for samples 11GV23, 11GV02 and 11GV05), average T was calculated for samples 11GV23 and 11GV05. Samples 11GV02 was probably in disequilibrium and no results were obtained from THERMOCALC. The temperatures of 510±61˚C and 474±43˚C for 11GV23 and 11GV05 are consistent with a retrograde fluid controlled overprint (see below).

Geochemistry

The whole rock geochemical analyses showed extremely high concentration of Ba in the NDZ, between 2000 to 7000 ppm. Among the major elements there were also high concentrations of Mn and Fe and possibly lower concentrations of Si in the NDZ (Fig. 20). From the EMPA analyses, Ba was found in K-feldspar and micas in the NDZ in two samples (11GV36 and 11GV38). High Mn concentrations were found in all the analysed garnets in the NDZ. This could indicate a different lithology in the NDZ. However, trace element data (Fig. 19) fit well with the North American shale composite (NASC) except for Ba; therefore it is plausible that the samples from NDZ and outside the NDZ are of similar origin. The high concentration of Ba is an indicator of fluid mobility (Grapes 1993). Therefore I suggest metasomatism where Ba, Mn and Fe were channelled along the deformation zone by fluids and reacted with the bedrock. This modified the bulk composition of the rocks in the NDZ by increasing the Ba, Mn and Fe concentrations and a possible loss of Si. Metasomatism occurred before and/or during the regional metamorphic event (Fig. 22). It cannot be excluded that metasomatism could have happened before the regional metamorphism as the age and earlier activities of the NDZ is uncertain (Bergman et al. 2001), however the most likely scenario is that metasomatism occurred during the regional metamorphism. The origin of this fluid could be from underlying metamorphosed mafic metasediments rich in Ba, Mn and Fe (Fig. 2). The underlying rocks experienced continental rifting from 2.5 -1.9 Ga which included mafic intrusions and epicontinental sedimentation (Weihed et al. 2005).

It is probable that several hydrothermal events occurred along the NDZ. A second event involving fluid interaction was visible in thin-section with retrograde reactions discussed in the petrology section above e.g. chlorite replacing garnet. Replacement of garnet by chlorite indicates that this fluid event occurred after the regional metamorphic event. The relative timing of the contact metamorphic event is more uncertain.

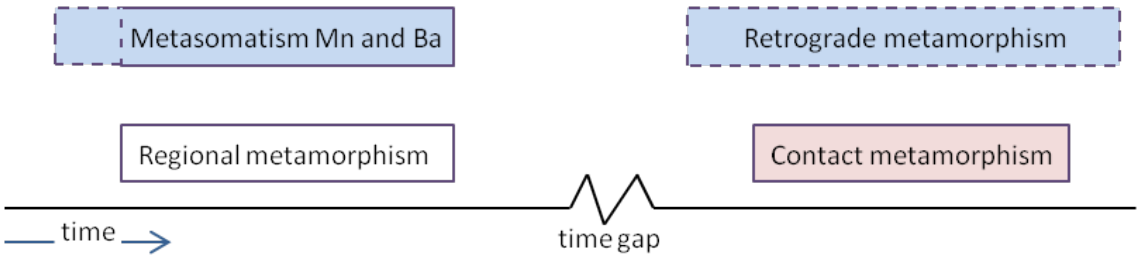

Fig. 22 Suggested time path for the metamorphic events in the Nautanen area: Blue rectangles indicate events in the NDZ; red rectangles indicate events close to the granite; white rectangles indicate events affecting the Nautanen area. The dotted rectangles are uncertain in their time positions.

Uncertainties

A number of uncertainties should be taken into account in the study. The standard deviations for the analyses (XRF, EMPA, point-counting and THERMOCALC) can be found in the appendix.

For the THERMOCALC calculation there are specific uncertainties that have to be mentioned: Propagation of errors from mineral analyses (e.g. heterogeneity in minerals and microprobe errors), poorly known activity–composition relationship (e.g. in this study Mn end-members) and errors in thermodynamic data (Powell and Holland 1994). The average PT calculation use the least-squares method to average the P and T. The uncertainties for the activities of the end members and their correlation are considered and given in table 3.

Conclusion

Based on petrographic analysis, P-T modelling using THERMOCALC and geochemical analysis, I propose that the Nautanen area has experienced:

- A regional metamorphic event with peak metamorphic temperatures ranging from 589 ±41˚C and 620 ±39˚C and pressures from 4±2.6 kbar and 4.3 ±1.5 kbar.
- Metasomatism in the NDZ with Ba, Mn and Fe rich fluids.
- Contact metamorphism in areas close to the granite intrusion. Temperatures and pressures for this event were estimated to 668 ±40˚C and 3.3 ±1.3 kbar in the NDZ, and 681 ±14˚C and 2.5 ±0.2 kbar east of the NDZ.
- Retrograde metamorphism at temperatures ranging from 474±43˚C and 510±61˚C for a pressure of 3 and 3.5 kbar in the NDZ caused by fluid flow channelled along the NDZ.

Acknowledgements

I would like to thank you supervisor Alasdair Skelton for his valuable support. I also thank you supervisors Stefan Bergman and Christina Wanhainen. I am very thankful to Dan Zetterberg, Rune Jacobsson, Marianne Ahlbom, Jarek Majka, Josefin Linde, Per-Olof Persson, Carina Johansson and Barbara Kleine for their help and assistance with sample preparation and analyses. Thank you to Hildred Crill for help to improve my English. Finally I would like to express my heartfelt thanks to all the staff and students at the Department of Geological Sciences.

References

Bergman S., Kübler L., Martinsson O., (2001) Description of regional geological and geophysical maps of northern Norrbotten county (east of the Caledonian orogen), *Sveriges geologiska undersökning,* Ba56

Condie K.C., (1993) Chemical composition and evolution of the upper continental crust: contrasting results from surface samples and shales, *Chemical Geology,* **104***,* 1-37

Ferry J. M., (2000) Patterns of mineral occurrence in metamorphic rocks, *American Mineralogist,* **85**, 1573–1588

Geijer P., (1918a) Nautanenområdet, en malmgeologisk undersökning, *Sveriges geologiska undersökning C 283*, 104 pp

Gieré R., Sorensen S. S., (2004) Allanite and other REE-rich epidote-group minerals, *Epidotes. Reviews in Mineralogy and Geochemistry*, **56**, 431–493.

Grapes R. H., (1993) Barian mica and distribution of barium in metacherts and quartsofeldspatic schists, Southern Alps, New Zealand, *Mineralogical Magazine*, **57**, 265-272

Holdaway M. J., Biswajit Mukhopadhyay, (1993) A reevaluation of the stability relations of andalusite: Thermochemical data and phase diagram for the aluminium silicates, *American Mineralogist,* **78**, 298-315

Holland T. J. B., Powell R., (1998) An internally consistent thermodynamic data set for phases of petrological interest, *Journal of Metamorphic Geology,* **16**, 309–343

Janots E., Engi M., Berger A., Allaz J., Schwarz J-O., Spandler C. (2008) Prograde metamorphic sequence of REE minerals in pelitic rocks of the Central Alps: implications for allanite–monazite–xenotime phase relations from 250 to 610 °C, *Journal of Metamorphic Geology,* **26**, 509–526

Lahtinen R., Korja A., Nironen M., (2005). Paleoproterozoic tectonic evolution, *Developments in Precambrian Geology*, **14**, 481-531

Martinsson O., Wanhainen C., (2004) Character of Cu-Au mineralizations and related hydrothermal alterations along the Nautanen deformation zone, Gällivare area, northern Sweden, *Society of Economic Geologists*, 149–160, *Society of Economic Geologists Guidebook Series*, nr 33

Mellqvist C., Öhlander B., Skiöld T., Wikström A., (1999) The Archaean–Proterozoic Palaeoboundary in the Luleå area, northern Sweden: field and isotope geochemical evidence for a sharp terraine boundary, *Precambrian Research,* **96**, 225–243

Öhlander B., Mellqvist C., T. Skiöld T., (1999) Sm–Nd isotope evidence of a collisional event in the Precambrian of northern Sweden, *Precambrian Research*, **93**, 105–117

Powell R., Holland T. J. B., (1988) An internally consistent dataset with uncertainties and correlations: 3. Applications to geobarometry, worked examples and a computer program, *Journal of Metamorphic Geology ,* **6**, 173–204

Powell R., Holland T. J. B., (1994) Optimal geothermometry and geobarometry, *American Mineralogist,* **79***, 120-133*

Powell R., Holland T. J. B., Worley B., (1998) Calculating phase diagrams involving solid solutions via non-linear equations, with examples using THERMOCALC, *Journal of Metamorphic Geology,* **16***, 577-588*

Skiöld T., (1987) Aspect of the Proterozoic Geochronology of Northern Sweden*, Precambrian Reasearch*, **35**, 161-167

Skiöld, T., Cliff, R.A., (1984) Sm-Nd and U-Pb dating of Early Proterozoic mafic-felsic volcanism in northernmost Sweden, *Precambrian Research,* **26***,* 1–13

Smith M. P., Storey C. D., Jeffries T. E., Ryan C., (2009) In Situ U-Pb and Trace Element Analysis of Accessory Minerals in the Kiruna District, Norrbotten, Sweden: New Constraints on the Timing and Origin of Mineralization, *Journal of Petrology,* **50**, 2063-2094

Symmes G. H., Ferry J. M.,(1992) The effect of whole-rock MnO content on the stability of garnet in pelitic schists during metamorphism, *Journal of Metamorphic Geology*, **10**, 221-237

van der Plas L., Tobi A. C., (1965) A chart for judging the reliability of point counting results, *American Journal of Science,* **263**, 87-90

Vernon R. H., (1988) Sequential growth of cordierite and andalusite porphyroblasts, Cooma Complex, Australia: microstructural evidence of a prograde reaction, *Journal of Metamorphic Geology* , **6**, 255-269

Wanhainen C., Broman C., Martinsson O., Magnor B., (2012) Modification of a Palaeoproterozoic porphyry-like system: Integration of structural, geochemical, petrographic, and fluid inclusion data from the Aitik Cu–Au–Ag deposit, northern Sweden. *Ore Geology Reviews,* **48**, 306–331

Weihed P., Arndt N., Billström K., Duchesne J-C., Eilu P., Martinsson O., Papunen H., Lahtinen R., (2005) Precambrian geodynamics and ore formation: The Fennoscandian Shield. *Ore Geology Reviews*, **27**, 273–322

Wing B. A., Ferry J. M., Harrison M. T., (2003) Prograde destruction and formation of monazite and allanite during contact and regional metamorphism of pelites: petrology and geochronology, *Contributions to Mineralogy and Petrology*, **145**, 228–250

Winkler, H.G.F., (1979) Petrogenesis of metamorphic rocks. *Springer Verlag, New York, Heidelberg, Berlin*, 348 pp

Witschard, F., (1996) Berggrundskartan 28K Gällivare, 1:50 000. *Sveriges geologiska undersökning, Ai 98–101*.

Zweifel, H., (1976) Geological documentation of a disseminated copper deposit - A preliminary investigation. *Sveriges geologiska undersökning C 720,* 80 pp

Appendix

Appendix A

Localities with coordinates and samples number

Locality 1	67 06'28,06''N 20 58'25,51''E
samples	11GV01, 11GV02
Locality 2	67 09'35,43''N 20 57'37,38''E
samples	11GV03, 11GV04
Locality 3	67 11'04,16''N 20 53'12,84''E
sample	11GV05
Locality 4	67 11'44,50''N 20 49'31,19''E
samples	11GV06, 11GV07, 11GV37
Locality 5	67 11'18,31''N 20 53'16,66''E
samples	11GV08, 11GV24
Locality 6	67 08'35,25''N 20 54'45,50''E
samples	11GV09, 11GV10, 11GV11, 11GV12, 11GV13
Locality 7	67 10'08,13''N 20 56'36,87''E
samples	11GV14, 11GV15
Locality 8	67 10'18,13''N 20 56'48,17''E
sample	11GV16
Locality 9	67 08'25,89''N 20 54'34,36''E
sample	11GV17
Locality 10	67 11'39,02''N 20 50'02,49''E
sample	11GV18
Locality 11	67 11'06,08''N 20 52'54,07''E
samples	11GV19, 11GV20, 11GV21, 11GV23
Locality 12	67 10'32,26''N 20 56'30,43''E
sample	11GV25
Locality 13	67 11'43,19''N 20 57'49,82''E
samples	11GV27, 11GV28
Locality 14	67 09'35,58''N 20 54'50,87''E
samples	11GV29, 11GV30
Locality 15	67 09'56,29''N 20 52'28,61''E
samples	11GV31, 11GV32, 11GV33
Locality 16	67 11'41,43''N 20 49'46,40''E
sample	11GV34
Locality 17	67 14'52,97''N 20 49'48,87''E
samples	11GV35, 11GV36
Locality 18	67 11'37,89''N 20 52'20,73''E
samples	11GV38, 11GV39, 11GV40, 11GV41

Endmember abbreviations

albite	ab	Fe-celadonite	fcel
almandine	alm	Fe-cordierite	fcrd
amesite	ames	grossular	gr
andalusite	and	Mn-cordierite	mncrd
andradite	andr	muscovite	mu
annite	ann	paragonite	pa
anorthite	an	phlogopite	phl
celadonite	cel	pyrope	py
clinochlore	clin	quartz	q
cordierite	crd	sanidine	san
daphnite	daph	sillimanite	sil
eastonite	east	spessartine	spss
epidote	ep	zoisite	zo

Loss on ignition

Sample (label)	Crucible weight (g)	Sample weight (g)	Crucible + Sample weight (g)	105°C 10h weight (g)	LOI 105°C weight (g)	1000°C 10h weight (g)	LOI 1000°C (g)	LOI tot weight (g)	LOI tot %
11GV02	25,6016	5,0853	30,6869	30,6843	0,0026	30,6449	0,0394	0,042	0,83%
11GV05	23,0364	5,1614	28,1978	28,1933	0,0045	28,0283	0,165	0,1695	3,28%
11GV06	24,9104	4,522	29,4324	29,4287	0,0037	29,3388	0,0899	0,0936	2,07%
11GV07	23,5178	4,8897	28,4075	28,4028	0,0047	28,3118	0,091	0,0957	1,96%
11GV08	24,9222	5,1244	30,0466	30,0378	0,0088	29,9263	0,1115	0,1203	2,35%
11GV12	22,8473	4,8827	27,73	27,7189	0,0111	27,6645	0,0544	0,0655	1,34%
11GV13	23,0097	5,0944	28,1041	28,0962	0,0079	28,0652	0,031	0,0389	0,76%
11GV14	25,3984	4,969	30,3674	30,364	0,0034	30,3039	0,0601	0,0635	1,28%
11GV17	23,0453	5,1071	28,1524	28,1419	0,0105	28,0369	0,105	0,1155	2,26%
11GV19	25,2621	5,0023	30,2644	30,2616	0,0028	30,1957	0,0659	0,0687	1,37%
11GV21	25,4972	5,4656	30,9628	30,9601	0,0027	30,9145	0,0456	0,0483	0,88%
11GV23	23,0025	5,0911	28,0936	28,0873	0,0063	27,9964	0,0909	0,0972	1,91%
11GV24	23,8843	5,0425	28,9268	28,9228	0,004	28,8086	0,1142	0,1182	2,34%
11GV25	22,7506	5,1698	27,9204	27,9168	0,0036	27,7989	0,1179	0,1215	2,35%
11GV27	25,2709	4,848	30,1189	30,1142	0,0047	30,0557	0,0585	0,0632	1,30%
11GV28	23,3613	5,2013	28,5626	28,5583	0,0043	28,4891	0,0692	0,0735	1,41%
11GV29	24,5403	5,1931	29,7334	29,7312	0,0022	29,4122	0,319	0,3212	6,19%
11GV33	24,8513	5,1005	29,9518	29,9469	0,0049	29,8465	0,1004	0,1053	2,06%
11GV35	24,0691	5,4812	29,5503	29,547	0,0033	29,5061	0,0409	0,0442	0,81%
11GV36	23,3198	4,826	28,1458	28,1398	0,006	28,1172	0,0226	0,0286	0,59%
11GV38	22,9085	5,0218	27,9303	27,9285	0,0018	27,88	0,0485	0,0503	1,00%

EMPA analyses for REE in allanite, sample 11GV07

Spot	A	B	C
F	0	0	0
Na2O	0,0267	0,0183	0,0158
As2O5	0	0	0
K2O	0,0017	0,0017	0,0111
SiO2	35	33,94	34,83
Al2O3	20,42	19,99	20,94
MgO	1,2784	1,3804	1,1474
ThO2	0,0017	0	0,0027
UO2	0	0,0154	0
P2O5	0,0207	0,0127	0,0106
CaO	15,96	15,38	16,89
La2O3	3,27	3,66	2,74
Ce2O3	6,27	6,75	5,38
Sm2O3	0,4171	0,4356	0,3815
Eu2O3	0	0	0
Gd2O3	0,1793	0,2294	0,2053
Nd2O3	2,23	2,5	2,09
Dy2O3	0,1674	0,11	0,0784
PbO	0	0,0023	0
TiO2	0	0	0
Y2O3	0,2649	0,339	0,2541
Pr2O3	0,6282	0,6805	0,5666
Er2O3	0,0253	0	0
Tb2O3	0	0	0
Ho2O3	0,0356	0,0223	0
Tm2O3	0	0	0
Yb2O3	0	0	0
Lu2O3	0,0118	0,0166	0,0275
FeO	9,71	9,38	9,61
MnO	1,0184	1,0755	0,9515
Total	96,9373	95,9397	96,1325

EMPA analyses

Sample	Na2O	Al2O3	SiO2	MgO	CaO	MnO	K2O	TiO2	Cr2O3	FeO	BaO	Total
11GV36												
garnet core	0	20,85	36,41	1,77	1,356	9,43	0,011	0	0,021	30,71	0	100,6
garnet rim	0,047	21,2	36,47	1,628	1,309	9,36	0,008	0,008	0,008	30,91	0	100,9
K feldspar	1,343	18,93	61,91	0,011	9E-04	0	13,57	0,06	0	0,11	2,42	98,35
biotite	0,077	18,27	34,81	6,9	0,014	0,215	9,28	3,41	0,026	23,46	0,38	96,84
muscovite	0,401	34,74	44,87	0,517	0,081	0,02	10,19	0,603	0,026	2,77	0,748	94,97
K-feldspar	1,57	18,97	62,08	0,031	0,021	0	13,26	0,054	0,01	0,171	2,51	98,68
11GV28												
biotite	0,201	19,58	35,07	8,23	0,033	0,125	9,21	2,59	0,022	20,44	—	95,5
muscovite	0,475	35,92	45,47	0,515	0	0,038	10,47	0,536	0	0,885	—	94,31
plagioclase*	8,28	19,86	69,14	0	2,75	0	0	0	0	0	—	100
sillimanite	0,024	62,88	37,09	0	0,03	0,027	0,019	0,013	0,06	0,173	—	100,3
andalusite	0,002	62,97	36,86	0,021	0,01	0,054	0,005	0,042	0,038	0,323	—	100,3
11GV25												
cordierite	0,204	33,56	48,47	10,53	0,002	0,557	0	0	0	4,26	0	97,58
biotite	0,353	19,44	36,5	14,84	0,006	0,144	8,91	1,169	0,064	12,61	0	94,04
plagioclase	8,57	24,15	61,21	0,009	5,29	0	0,043	0,033	0	0,263	0	99,57
chlorite	0,007	23,58	25,61	21,56	0,045	0,316	0	0,101	0	15,76	0	86,98
muscovite*	1,64	35,15	51,6	1,37	0	0	8,44	0	0	1,8	0	100
11GV02												
plagioclase	7,73	25,48	59,02	0	6,82	0,013	0,111	0,043	0,019	0,288	—	99,52
biotite	0,03	17,34	36,26	12,58	0,105	0,825	9,45	1,86	0,033	15,53	—	94,01
K-feldspar	0,212	18,62	63,88	0,031	0,041	0	16,2	0,039	0	0,208	—	99,23
garnet rim	0,044	20,44	36,09	0,952	5,58	26,07	0,014	0,161	0,053	11,07	—	100,5
garnet core	0,013	20,73	36,37	1,018	5,55	25,41	0	0,143	0,029	11,06	—	100,3
11GV38												
garnet core	0,023	20,5	36,46	1,156	2,65	18,13	0,001	0,041	0	20,74	—	99,7
garnet rim	0,003	21,04	36,69	0,922	4,65	17,38	0,021	0,046	0,026	19,96	—	100,7
biotite	0,036	16,69	34,84	7,94	0,001	0,544	9,26	3,17	0	23,02	—	95,5
Muscovite	0,226	31,99	44,37	0,741	0	0,049	10,5	0,979	0,026	4,3	—	93,18
K-feldspar*	0,8	18,2	62,91	0	0	0	12,45	0	0	2,37	3,27	100
11GV23												
epidote rim	0,015	22,24	36,57	0	23,66	0,039	0,022	0,154	0,025	13,24	—	95,96
epidote core	0,033	29,76	37,25	0	23,86	0,148	0	0,02	0	3,11	—	94,18
biotite	0,075	17,49	33,12	6,46	0,032	0,449	8,91	0,94	0	26,62	—	94,1
muscovite	0,184	35,38	45,85	0,491	0,231	0,118	9,2	0,006	0	0,835	—	92,3
garnet rim	0	20,95	36,39	0,975	7,43	10,86	3E-04	0	0	23,1	—	99,71
garnet core	0,113	21,13	35,26	0,279	2,42	24,94	0,015	0,068	0,019	15,77	—	100
11GV07												
muscovite	0,191	1,501	31,65	48,14	0	0,002	10,43	0,348	0,049	5,239	—	97,55
epidote	0,067	0,067	23,72	37,77	22,93	0,633	0,019	0,047	0,044	11,29	—	96,58

K-feldspar	0,428	0,024	18,42	64,9	0	0,017	16,15	0	0	0,057	—	99,99
11GV05												
garnet rim	0,018	19,17	37,34	0,892	11,76	19,61	0,01	0,182	0,047	10,87	—	99,9
chlorite	0,017	18,67	28,75	21,09	0,015	1,062	0,021	0,028	0	17,26	—	86,91
epidote	0	22,5	36,86	0	22,67	0,622	0	0,02	0,002	12,48	—	95,15
K-feldspar	0,657	18,42	62,32	0,038	0	0,083	14,49	0,1	0,029	0,256	—	96,39
garnet core	0,053	18,78	36,71	0,618	5,46	28,83	0,013	0,52	0,04	8,56	—	99,58

* Mineral analyses from SEM

Elements and calibration standard for EMPA

Element	Standard
Na	Albi ($NaAlSi_3O_8$)
Al	Al_2O_3
Si	Wollastonite ($CaSiO_3$)
Mg	MgO
Ca	Wollastonite ($CaSiO_3$)
Mn	Pyrophanite ($MnTiO_3$)
K	Orhtoclase ($KAlSi_3O_8$)
Ti	Pyrophanite ($MnTiO_3$)
Cr	Cr_2O_3
Fe	Fe

Appendix B

XRF analyses

		11GV02	11GV05	11GV06	11GV07	11GV08	11GV12	11GV13
SiO2	mass%	55,51	46,74	73,84	73,49	51,38	64,03	65,25
Al2O3	mass%	19,39	22,66	13,96	13,50	18,37	16,01	16,52
CaO	mass%	3,53	8,06	0,85	0,87	4,40	2,42	2,01
MgO	mass%	1,58	4,13	1,94	2,24	3,75	2,48	1,78
MnO	mass%	0,43	1,91	0,05	0,07	2,00	0,13	0,08
P2O5	mass%	0,20	0,23	0,01	0,01	0,17	0,13	0,14
Fe2O3	mass%	11,18	9,79	3,54	3,93	14,47	7,52	5,66
Na2O	mass%	4,87	0,64	0,15	0,19	0,15	5,50	6,47
K2O	mass%	2,62	5,29	5,45	5,51	4,89	1,19	1,51
TiO2	mass%	0,70	0,54	0,19	0,20	0,42	0,59	0,59
Total		100,00	100,00	100,00	100,00	100,00	100,00	100,00
Ce	ppm	80	51	77	88	43	51	54
La	ppm	45	29	38	45	26	24	35
Th	ppm	5	8	14	11	6	12	11
Ni	ppm	0	0	7	7	6	23	19
V	ppm	105	131	36	31	119	86	84
Ba	ppm	372	5012	815	885	3151	300	555
Cr	ppm	17	46	17	16	46	79	76
Cu	ppm	0	0	0	0	0	238	11
Ga	ppm	23	17	21	18	13	20	21
Hf	ppm	4	4	4	4	3	7	5
Nb	ppm	15	7	17	15	6	8	8
Pb	ppm	4	6	3	3	3	4	2
Rb	ppm	110	265	211	222	263	52	47
Sr	ppm	308	525	41	47	173	140	257
Y	ppm	16	16	21	28	18	16	12
Zr	ppm	272	103	135	129	77	167	176

		11GV14	11GV17	11GV19	11GV21	11GV23	11GV24	11GV25
SiO2	mass%	54,87	62,16	58,28	52,50	40,70	53,51	62,21
Al2O3	mass%	19,20	14,32	17,36	19,03	19,27	19,80	18,12
CaO	mass%	4,68	7,13	4,15	3,63	2,80	4,01	1,35
MgO	mass%	2,85	2,48	1,78	1,88	4,19	3,09	2,92
MnO	mass%	0,13	0,23	0,83	0,86	1,68	0,43	0,08
P2O5	mass%	0,25	0,12	0,25	0,18	0,15	0,18	0,15
Fe2O3	mass%	9,43	8,80	10,37	15,25	24,32	11,87	8,97
Na2O	mass%	5,24	0,26	1,74	3,12	0,07	0,37	1,97
K2O	mass%	2,56	3,82	4,58	3,13	6,32	6,29	3,40
TiO2	mass%	0,80	0,69	0,67	0,42	0,50	0,44	0,83
Total		100,00	100,00	100,00	100,00	100,00	100,00	100,00

Ce	ppm	90	82	85	51	114	30	75
La	ppm	43	55	49	24	80	31	44
Th	ppm	7	8	7	7	3	4	15
Ni	ppm	2	30	5	6	0	4	56
V	ppm	185	107	131	251	108	134	149
Ba	ppm	1491	333	2763	2215	4591	7204	719
Cr	ppm	37	172	29	46	40	73	168
Cu	ppm	0	21	21	37	65	0	0
Ga	ppm	20	20	18	14	7	16	25
Hf	ppm	5	3	3	5	2	3	4
Nb	ppm	8	7	9	6	6	6	15
Pb	ppm	5	5	5	2	3	11	6
Rb	ppm	55	170	175	122	374	278	127
Sr	ppm	645	109	225	222	81	220	141
Y	ppm	19	22	20	14	31	11	29
Zr	ppm	159	125	147	81	66	81	151

		11GV27	11GV28	11GV29	11GV33	11GV35	11GV36	11GV38
SiO2	mass%	62,32	62,72	48,27	66,21	60,28	54,09	68,00
Al2O3	mass%	19,85	18,95	18,71	14,17	19,31	17,99	12,15
CaO	mass%	0,58	0,61	10,81	5,01	2,20	0,59	0,45
MgO	mass%	2,84	2,89	2,25	3,46	0,93	0,97	0,51
MnO	mass%	0,07	0,06	1,05	0,13	0,30	0,82	0,52
P2O5	mass%	0,10	0,08	0,18	0,10	0,15	0,26	0,15
Fe2O3	mass%	8,22	8,06	11,39	6,12	6,70	18,97	12,91
Na2O	mass%	0,91	1,70	0,33	0,94	1,30	0,37	0,05
K2O	mass%	4,30	4,11	6,55	3,26	8,27	5,39	4,76
TiO2	mass%	0,82	0,83	0,45	0,61	0,58	0,55	0,49
Total		100,00	100,00	100,00	100	100,00	100,00	100,00
Ce	ppm	81	77	30	41	87	88	6
La	ppm	49	38	23	13	58	60	7
Th	ppm	16	14	5	11	18	18	6
Ni	ppm	50	59	0	39	0	0	0
V	ppm	139	142	150	92	91	104	214
Ba	ppm	483	660	3002	751	6272	6266	4940
Cr	ppm	138	143	27	94	73	52	50
Cu	ppm	32	15	0	0	40	95	56
Ga	ppm	27	24	13	20	19	21	17
Hf	ppm	3	7	1	3	6	2	3
Nb	ppm	15	15	6	11	14	23	7
Pb	ppm	3	3	5	4	7	6	2
Rb	ppm	192	152	208	170	285	244	131
Sr	ppm	34	49	284	266	241	168	149

Y	ppm	28	26	12	23	23	24	11
Zr	ppm	151	141	71	155	291	282	109

USGS standards disque (AGV 2) is analysed as an unknown every 6th samples.

Expected standard values and the deviation from the standard values.

	SiO2	Al2O3	CaO	MgO	MnO	P2O5	Fe2O3	Na2O	K2O	TiO2
mass%	60,15	17,15	5,27	1,82	0,10	0,49	6,79	4,25	2,92	1,07
sd	0,00	0,00	0,01	0,02	0,01	0,38	0,00	0,01	0,00	0,01

	Ce	La	Th	Ni	V	Ba	Cr	Cu	Ga	Hf
ppm	68	38	6	19	120	1140	17	53	20	5
sd	0,05	0,03	0,04	0,05	0,01	0,01	0,16	0,01	0,02	0,18

	Nb	Pb	Rb	Sr	Y	Zr
ppm	15	13	69	658	20	230
sd	0,07	0,07	0,01	0,01	0,07	0,01

Appendix C

Condensed THERMOCALC output

Sample 11GV25

	phl	ann	east	clin	daph	ames	crd
a	0,126	0,0087	0,111	0,132	0,00172	0,13	0,69
sd(a)/a	0,24964	0,56786	0,2668	0,24322	0,69725	0,24533	0,05

	fcrd	ab	mu	pa	q	H2O	and
a	0,03	0,75	0,5	0,64	1	1	1
sd(a)/a	0,41015	0,05	0,1	0,05	0	0	

Reactions and calculations for x(H2O) = 1,0	P(T)	sd(P)
1) 2phl + mu + 2and = 3east + 5q	2,8	5,45
2) 5fcrd + 11pa = 2daph + 11ab + 3H2O + 19and	0,41	11,75
3) 2phl + 3fcrd = 2ann + 3crd	9,9	59,58
4) 4phl + 3daph + mu + 2and = 5ann + 3ames + 5q	11,2	15,28
5) 2east + 2clin + 3fcrd = 2ann + 2ames + 3crd	17,7	15,43
6) 29phl + crd + 36pa = 22east + 9clin + 36ab + 7mu	4	1,82
7) 8east + 2clin + 8ab + 7q = 8phl + crd + 8pa	3,7	2,49

Single end-member diagnostic information (e* cutoff = 2,50; hat cutoff = 0,50; fit cutoff = 1,49)

	P	sd(P)	T	sd(T)	cor	fit	e*	hat
phl	4,26	2	587	54	0,994	1,4	0,06	0,48
ann	4,41	1,52	591	41	0,989	1,38	-0,5	0,02
east	4,19	1,57	585	42	0,99	1,38	0,47	0,09
clin	4,52	1,39	591	37	0,987	1,27	-1,25	0,19
daph	4,42	1,46	591	39	0,989	1,34	0,79	0,02
ames	4,64	1,11	601	30	0,988	1,01	2,1	0,18
crd	4,09	1,64	583	43	0,988	1,38	-0,32	0,2
fcrd	4,31	1,49	588	40	0,989	1,37	-0,63	0,02
ab	4,23	1,43	584	39	0,987	1,31	0,85	0,16
mu	4,2	1,84	585	50	0,993	1,39	-0,11	0,17
pa	4,23	1,43	584	39	0,987	1,31	-0,85	0,16
q	4,34	1,52	589	41	0,989	1,4	0	0
H2O	4,34	1,52	589	41	0,989	1,4	0	0
and	4,34	1,52	589	41	0,989	1,4	0	0

Sample 11GV28

	phl	ann	east	mu	cel	fcel	pa
a	0,03	0,06	0,034	0,79	0,0091	0,0088	0,202
sd(a)/a	0,4102	0,3333	0,3991	0,1	1,0989	1,1364	0,191

	ab	q	H2O	and	sill
a	0,85	1	1	1	1
sd(a)/a	0,05	0	0	0	

Reactions and calculations for x(H2O) = 1,0	P(T)	sd(P)
1) sill = and	3,7	0,22
2) 2phl + mu + 2sill = 3east + 5q	7,7	6,41
3) phl + cel + 2and = 2east + 5q	8,1	6,7
4) 3east + 3fcel = 2phl + ann + 3mu	3,4	29,54
5) 3fcel + 2pa = ann + 2mu + 2ab + 3q + 2H2O	2,4	4,89

Single end-member diagnostic information (e* cutoff = 2,50; hat cutoff = 0,42; fit cutoff = 1,61)

	P	sd(P)	T	sd(T)	cor	fit	e*	hat
phl	2,49	0,22	682	14	-0,475	0,56	0,58	0
ann	2,49	0,22	681	14	-0,474	0,7	-0,02	0
east	2,48	0,22	682	14	-0,475	0,45	-0,93	0
mu	2,49	0,22	681	14	-0,474	0,7	0,04	0
cel	2,49	0,22	681	14	-0,474	0,66	0,44	0
fcel	2,49	0,22	681	14	-0,474	0,69	0,2	0
pa	2,53	0,37	679	26	-0,822	0,69	-0,07	0,92
ab	2,49	0,24	681	15	-0,537	0,7	0,02	0,06
q	2,49	0,22	681	14	-0,474	0,7	0	0
H2O	2,49	0,22	681	14	-0,474	0,7	0	0
and	2,49	0,22	681	14	-0,474	0,7	0	0
sill	2,49	0,22	681	14	-0,474	0,7	0	0

Sample 11GV38

	phl	ann	east	py	alm	mu	cel
a	0,0223	0,099	0,02	0,00017	0,089	0,63	0,0104
sd(a)/a	0,43418	0,25991	0,44229	0,80305	0,27575	0,1	0,96154

	pa	san	ab	q	H2O
a	0,088	0,93	0,378	1	1
sd(a)/a	0,24952	0,05	0,11607	0	

Reactions and calculations for x(H2O) = 1,0	P(T)	sd(P)
1) 3east + 6q = phl + py + 2mu	3,7	3,48
2) phl + east + 6q = py +2cel	4,3	4,02
3) phl + alm = ann + py	6,4	25,2
4) east + cel + ab = phl + pa + san	11,2	30
5) py + 3cel + 2pa = 3east + 2ab + 9q + 2H2O	3,7	2,87

Single end-member diagnostic information (e* cutoff = 2,50; hat cutoff = 0,42; fit cutoff = 1,61)

	P	sd(P)	T	sd(T)	cor	fit	e*	hat
phl	4	2,64	620	39	0,837	0,28	0,05	0,11
ann	3,99	2,6	618	44	0,817	0,28	-0,09	0,26
east	4,19	3,41	622	47	0,899	0,28	0,05	0,46
py	4,22	2,72	625	44	0,868	0,26	-0,2	0,27
alm	3,99	2,6	618	44	0,815	0,28	0,09	0,29
mu	3,99	2,59	621	39	0,839	0,27	0,12	0,06
cel	3,81	3,07	618	44	0,882	0,28	0,13	0,4
pa	4,06	2,58	620	39	0,853	0,21	-0,35	0,01
san	4,04	2,58	621	40	0,839	0,28	-0,06	0,05
ab	4,05	2,58	620	39	0,854	0,25	0,16	0
q	4,03	2,58	620	39	0,855	0,29	0	0
H2O	4,03	2,58	620	39	0,855	0,29	0	0

Sample 11GV36

	phl	ann	east	py	alm	mu	cel
a	0,0168	0,095	0,019	0,00042	0,29	0,7	0,0094
sd(a)/a	0,45454	0,26606	0,44599	0,77025	0,15	0,1	1,06383

	pa	san	ab	q	H2O	sill
a	0,204	0,88	0,49	1	1	1
sd(a)/a	0,19008	0,05	0,07803	0	0	

Reactions and calculations for x(H2O)= 1,0	P(T)	sd(P)
1) 3east + 6q = phl + py + 2mu	5,7	3,48
2) phl + east + 6q = py + 2cel	6,1	4,35
3) 2phl + mu + 2sill = 3east + 5q	9,7	7,13
4) py + 2mu = phl + san + H2O + 3sill	1,4	2,19
5) ann + q + 2sill = alm + mu	2,6	1,25
6) east + cel + ab = phl + pa + san	1,8	32,03

Single end-member diagnostic information (e* cutoff = 2,50; hat cutoff = 0,46; fit cutoff = 1,54)

	P	sd(P)	T	sd(T)	cor	fit	e*	hat
phl	3,56	1,36	674	40	0,963	0,83	0,72	0,03
ann	3,31	1,74	667	52	0,978	0,93	-0,02	0,4
east	3,1	1,37	660	40	0,964	0,82	-0,9	0,05
py	3,59	1,5	675	44	0,97	0,91	-0,35	0,24
alm	3,33	1,53	667	45	0,971	0,93	0,01	0,13
mu	3,7	1,41	669	40	0,925	0,84	-0,59	0,59
cel	3,21	1,36	664	40	0,963	0,89	0,65	0,04
pa	3,27	1,34	670	40	0,954	0,79	0,98	0,2
san	3,32	1,34	664	41	0,948	0,9	0,29	0,16
ab	3,32	1,34	669	40	0,959	0,88	-0,4	0,03
q	3,35	1,34	668	40	0,962	0,93	0	0
H2O	3,35	1,34	668	40	0,962	0,93	0	0
sill	3,35	1,34	668	40	0,962	0,93	0	0

Sample 11GV07

	phl	ann	east	mu	cel	fcel	pa
a	0,35	0,0013	0,119	0,57	0,021	0,0122	0,054
sd(a)/a	0,1001	0,7125	0,2574	0,1	0,47619	0,8197	0,2685

	san	ab	q	H2O
a	0,96	0,216	1	1
sd(a)/a	0,05	0,1844	0	

Reactions and calculations at P = 3 kbar, for x(H2O) = 1	T(P)	sd(T)
1) east + cel = phl + mu	616	341
2) 3cel = phl + 2san + 3q + 2H2O	584	52
3) 3fcel = ann + 2san + 3q + 2H2O	311	106
4) 3fcel + 2pa = ann + 2mu + 2ab + 3q + 2H2O	281	101

Single end-member diagnostic information (e* cutoff = 2,50; hat cutoff = 0,36; fit cutoff = 1,61)

	T	sd	fit	e*	hat
phl	583	34	1,04	0,1	0,04
ann	586	29	0,95	0,5	0
east	565	49	1	-0,3	0,67
mu	582	36	1,04	0,1	0,09
cel	584	34	1,05	0	0,11
fcel	592	17	0,55	-1,7	0,03
pa	584	32	1,04	0,1	0
san	585	33	1,04	0	0,02
ab	584	32	1,04	0	0
q	584	32	1,05	0	0
H2O	584	32	1,05	0	0

Samples 11GV23

	phl	ann	east	py	gr	alm	mu
a	0,0112	0,085	0,02	0,000226	0,0111	0,11	0,79
sd(a)/a	0,47972	0,28256	0,44229	0,7937	0,54326	0,24416	0,10000

	cz	q	H2O
a	0,85	1	1,00
sd(a)/a	0,10588	0	

Reactions and calculations at P = 3 kbar, for x(H2O) = 1	T(P)	sd(T)
1) 15phl + 24cz = 15east + 5py + 16gr + 24q + 12H2O	523	137
2) phl + alm = ann + py	671	531
3) ann + 3east + 6q = 2phl + alm + 2mu	614	430

Single end-member diagnostic information (e* cutoff = 2,50; hat cutoff = 0,30; fit cutoff = 1,73)

	T	sd	fit	e*	hat
phl	495	66	0,71	0,5	0,11
ann	515	61	0,7	-0,4	0,01
east	510	61	0,82	0	0,02
py	491	66	0,59	-0,8	0,14
gr	554	94	0,7	0,4	0,64
alm	514	61	0,73	0,4	0,01
mu	511	61	0,82	0,1	0,01
cz	515	66	0,81	-0,1	0,05
q	510	61	0,82	0	0
H2O	510	61	0,82	0	0

Sample 11GV05

	clin	daph	ames	cz	ep	py	gr
a	0,12	0,0028	0,0586	0,21	0,73	0,00019	0,021
sd(a)/a	0,25631	0,66418	0,34467	0,36667	0,1	0,79949	0,4719

	alm	andr	q	H2O
a	0,0063	0,0605	1	1
sd(a)/a	0,59826	0,332	0	

Reactions and calculations at P = 3,5 kbar, for x(H2O) = 1	T(P)	sd(T)
1) clin + ames + 4q = 3py + 8H2O	478	34
2) 21clin + 24cz = 9ames + 23py + 16gr + 60H2O	530	44
3) 3clin + 5alm = 3daph + 5py	563	1794
4) 2cz + andr = 2ep + gr	670	269

Single end-member diagnostic information (e* cutoff = 2,50; hat cutoff = 0,36; fit cutoff = 1,61)

	T	sd	fit	e*	hat
clin	471	36	1,81	1,5	0
daph	475	48	2,21	-0,1	0,12
ames	484	30	1,48	-2,5	0,03
cz	473	42	2,16	0,8	0
ep	473	41	2,08	0,8	0
py	466	57	2,19	-0,4	0,56
gr	472	39	1,99	-1,3	0
alm	475	51	2,21	0,1	0,27
andr	473	38	1,96	-1,4	0
q	474	43	2,21	0	0
H2O	474	43	2,21	0	0